SLAC-PUB-5924 Rev.
February 1993
(E/T)

LASER + e^- $\rightarrow$ γ + e^-

AND

LASER + γ $\rightarrow$ e^+ + e^-

AS SOURCES OF PRODUCING

CIRCULARLY POLARIZED γ AND $e^\pm$ BEAMS*

Yung Su Tsai

Stanford Linear Accelerator Center

Stanford University, Stanford CA 94309, USA

ABSTRACT

Helicity amplitudes of reactions laser-electron scattering and laser + $\gamma \rightarrow e^+ + e^-$ are investigated. Mechanisms to produce nearly 100% circularly polarized γ and $e^\pm$ beams are discussed using the above mentioned reactions. Circularly polarized $e^\pm$ beams from circularly polarized γ's impinging upon an atomic target are also investigated.

Submitted to *Physical Review D*

---

*Work supported by Department of Energy contract DE-AC03-76SF00515.

1. Introduction

If positrons and electrons can be made circularly polarized and rendered to collide head on, interesting physics can be learned. Most spectacular would be observation of the nonzero annihilation cross section when the helicity of e^- is equal to that of e^+. This will imply the existence of a spin 0 or spin 2 particle coupled to the electron. Also in the interaction $e^+e^- \to \tau^+\tau^-$, $\tau^\pm$ can be made highly polarized; this will give us a handle to decide whether τ is coupled to the right-handed W and the charged Higgs particle in addition to the standard left-handed W. Polarized $\tau^\pm$ can also be used to test the CP violation in the τ decay.

In this paper we want to accomplish two goals. The first goal is to investigate the properties of the two reactions mentioned in the title[1,2]. The second is to consider the merits of using these two reactions as sources of polarized γ, e^+ and e^- beams. For the near term future, the best source of polarized $e^\pm$ beams will most likely be ordinary pair production of $e^\pm$ using the polarized photon from the first reaction. The reason is that for regular pair production, $\gamma + Z \to e^+e^- + Z + \cdots$, the threshold energy is only a few MeV and thus even a 20 MeV photon is sufficient to produce almost 100% polarized $e^\pm$ beams.

In contrast to this, the pair production using the second reaction requires a free electron laser (with photon energy > 15 eV) and a backward-scattered high energy γ of several tens of GeV. The advantage of the latter is that the transverse momentum of $P_\perp$ of $e^\pm$ is much smaller than m, whereas in ordinary pair production $P_\perp$ is caused mainly by the Coulomb multiple scatterings of $e^\pm$ in the target, which is given roughly by 14 MeV $\sqrt{t}$ where

t is the path length of $e^{\pm}$ in the target in units of radiation length of the target material. The transverse momentum $P_{\perp}$, as well as the spread of the longitudinal momentum ΔP_l of $e^{\pm}$ beam, can be greatly reduced by the cooling rings, so it is not obvious that the smallness of $P_{\perp}$ for $e^{\pm}$ produced by laser $+ \gamma \rightarrow e^+e^-$ has such a crucial advantage. Obviously, further detailed engineering studies must be carried out.

When the intensity of the laser beam becomes very high, the coherence of laser photons becomes important [2,3]. In fact if the intensity becomes so high that the dimensionless parameter (see Appendix A)

$$\xi^2 = 4\pi\alpha \left(\frac{a}{m}\right)^2 = n_\gamma \frac{2.71 \times 10^{-27}}{w_1(\mathrm{eV})} , \tag{1.1}$$

where n_γ = number of photons /cm^3 in the laser beam, w_1 = laser photon energy in eV, a=amplitude for the vector potential in radiation gauge, becomes comparable to one, then our treatment of the problem breaks down, because we assumed the convergence of a series expansion in ξ^2. The cross section is the sum of cross sections, $\sum \sigma_s$, each of which is produced by s coherent incident photons. Roughly speaking the σ_s is proportional to ξ^{2s}. Thus when $\xi^2 \sim 1$, $\sigma_1, \sigma_2, \sigma_3, \sigma_4 \cdots$ have almost the same magnitudes.

We follow the work of D. M. Volkov [1], who obtained the solution to the Dirac equation in the plane electromagnetic field in 1935, long before the invention of laser. Obviously, in order to apply his formalism to the laser photon-electron interaction, the laser beam must have a larger dimension than that of the electron beam, and the laser photon wave length must be short compared with the intersecting length of the electron beam inside the laser beam, in order to take the time-averaged value of electron momentum in the laser field, such as is done in Eq. (40.14) of Ref. [1].

For production of polarized γ and $e^{\pm}$ beams, the coherence effects of the laser beam [i.e., cross sections with s$\geq$2 in Eqs. (2.11) and (3.1)] have many undesirable effects. Roughly speaking, the high-energy tips (within $20 \sim 30\%$ from the very tip) of the spectra of both reactions have characteristics of high intensity and high polarization. The locations of the tips of the spectrum differ for each s as given by Eq. (2.34) for the reaction $sk_1 + p_1 \rightarrow k_2 + p_2$ and Eq. (3.30) for the reaction $sk_1 + k_2 \rightarrow p_1 + p_2$. The tip of the spectrum for the $s = 1$ case is the most important energy, but this point is somewhat below the energy tips for cross sections with $s \geq 2$. Thus the contributions from s$\geq$2 do not have good polarization characteristics near the tip of the spectrum for the $s = 1$ case for both reactions. When the center-of-mass energies are high compared with the mass of the electron [see Eqs. (2.34) and (3.30)] $u_{\max}$ approaches unity for all s's for both reactions, and the objectionable features of higher s contributions disappear. For low energies (i.e., when the center-of-mass energy is not relativistic), one should keep $\xi < 0.5$ and increase the laser pulse length in order to maintain good polarization and good intensity.

In Sec. 2 we treat the differential cross section and the polarization of the scattered photon k_2 for arbitrarily polarized k_1 and p_1 in the reaction laser $(sk_1) + p_1 \rightarrow k_2 + p_2$. Measurement of the electron polarization using polarized laser beams is discussed.

In Sec. 3 we treat the differential cross section and the polarization of $e^{\pm}$ from arbitrarily polarized k_1 and k_2 in the reaction laser $(sk_1) + k_2 \rightarrow e^+(p_1) + e^-(p_2)$.

In Sec. 4 we treat the energy distribution and the polarization of $e^{\pm}$ from an arbitrarily polarized (circular) photon in the reaction

$$k + Z \rightarrow e^{+}e^{-} + \cdots,$$

where Z is an atomic target (numerical examples given are for tungsten).

In Sec. 5 we summarize and discuss our results.

2. Laser-electron interactions.

We follow closely the work of Volkov, as given in Ref. [1]. In this section, we treat the interaction $sk_1 + p_1 \rightarrow k_2 + p_2$ (see Fig. 1).

Each electron and photon can have two helicity states, and thus there are altogether sixteen helicity amplitudes for each s. Let us denote each of this amplitude by $A_{s\lambda_1\lambda_2\lambda_3\lambda_4}$ where $\lambda_1, \lambda_2, \lambda_3$, and λ_4 are helicities of the incident photon, the outgoing photon, the outgoing electron, and the incident electron respectively. For example, A_{spnnp} means λ_1 is positive, λ_2 is negative, λ_3 is negative and λ_4 is positive. Because of the parity conservation, we have $A_{s\lambda_1\lambda_2\lambda_3\lambda_4} = A_{s,-\lambda_1,-\lambda_2,-\lambda_3,-\lambda_4}$; thus we need to calculate only eight helicity amplitudes, which we chose to be:

$$A_{snnnn}\,, \quad A_{snnnp}\,, \quad A_{snnpn}\,, \quad A_{snnpp}\,,$$

$$A_{snpnn}\,, \quad A_{snpnp}\,, \quad A_{snppn}\,, \quad A_{snppp}\,.$$

Our calculational strategy is the following: we choose the center-of-mass system to obtain expressions for $A_{s\lambda_1\lambda_2\lambda_3\lambda_4}$ and then evaluate these expressions in the coordinate system where the experiment is carried out. In the center-of-mass system, the expressions for $A_{s\lambda_1\lambda_2\lambda_3\lambda_4}$'s are the simplest.

The center-of-mass system we have used differs somewhat from the usual one, because of the presence of a laser field in which electrons not only acquire additional momentum in the direction of the laser beam but also an additional mass due to its helical motion in the laser field. Let us denote the four momenta of the laser photon, the outgoing photon, the incident electron, and the outgoing electron by k_1, k_2, p_1, and p_2 respectively. Let q_1 and q_2 be the quasi-four momenta of p_1 and p_2 electrons inside the laser field:

$$q_1 = p_1 + \frac{\xi^2 m^2}{2p_1 \cdot k_1} k_1 , \tag{2.1}$$

$$q_2 = p_2 + \frac{\xi^2 m^2}{2p_2 \cdot k_1} k_1 , \tag{2.2}$$

where ξ^2 is the dimensionless parameter representing the intensity of the laser defined in Appendix A.

From (2.1) and (2.2), we obtain the quasi-mass of the electrons in the laser field

$$q_1^2 = q_2^2 = m^2(1+\xi^2) \equiv m^{*2} .$$

The energy momentum conservation is

$$sk_1 + q_1 = k_2 + q_2 \tag{2.3}$$

or

$$(s-\eta)k_1 + p_1 = k_2 + p_2 \tag{2.4}$$

where

$$\eta = \frac{\xi^2 m^2}{2}\left(\frac{1}{p_2 \cdot k_1} - \frac{1}{p_1 \cdot k_1}\right) . \tag{2.5}$$

Our center-of-mass system is defined by

$$(s-\eta)\vec{k}_1 + \vec{p}_1 = \vec{k}_2 + \vec{p}_2 = 0 .$$

In this system, the four vectors k_1, k_2, p_1 and p_2 have the following components (see Fig 2)

$$k_1 = \left(\frac{p}{s-\eta}, 0, 0, \frac{p}{s-\eta}\right) , \tag{2.6a}$$

$$k_2 = (p, p\sin\theta, 0, p\cos\theta) , \tag{2.6b}$$

$$p_1 = (e, 0, 0, -p) , \tag{2.6c}$$

$$p_2 = (e, -p\sin\theta, 0, -p\cos\theta) . \tag{2.6d}$$

Since k_1 depends upon η in the coordinate system, we can substitute the expression for k_1 given above into Eq. (2.5) and solve for η. We obtain:

$$s - \eta = \frac{s}{1+\epsilon} , \tag{2.7}$$

with $\epsilon = \xi^2 m^2/2 \times (1-x)/[(e+p)(e+px)]$ and $x = \cos\theta$.

A tremendous number of cancellations occur in the course of calculation. Since p and e are related by $e^2 = p^2 + m^2$, the final expression cannot be unique if we treat e and p as independent variables. This is remedied by using the variable $y = (e+p)/m$. In terms of y, we have

$$e = \frac{m(y^2+1)}{2y} , \tag{2.8}$$

$$p = \frac{m(y^2-1)}{2y} . \tag{2.9}$$

We used the commercially available computer program [4] called MAPLE to obtain all our analytical expressions, as well as the numerical results. The helicity amplitudes were obtained by explicitly writing down spinors u, v as 4×1 arrays, $\bar{u}$ and $\bar{v}$ as 1×4 arrays, and by using explicit representations for all γ matrices. MAPLE handled all the matrix multiplications and simplifications (see Appendix B).

Let the vector potential representing the laser field be

$$\vec{A} = \vec{a}_1 \cos\Phi + \vec{a}_2 \sin\Phi, \tag{2.10}$$

where $\Phi = k_1 \cdot x = [p/(s-\eta)]\,(t-z)$. For $\lambda_1 =$ positive, we have

$$\vec{a}_1 = a\hat{e}_x \quad \text{and} \quad \vec{a}_2 = a\hat{e}_y \ ,$$

and for $\lambda_1 =$ negative, we have

$$\vec{a}_1 = a\hat{e}_x \quad \text{and} \quad \vec{a}_2 = -a\hat{e}_y \ ,$$

where a is defined by Eq. (1.1).

The matrix element for laser photon-electron scattering—see Eq. (101.9) of Ref. [1]—can be written

$$(S_{fi})_{\lambda_1\lambda_2\lambda_3\lambda_4} = \frac{-ie}{\sqrt{8q_{10}q_{20}k_{20}}}\,(2\pi)^4 \sum_{s=1}^{\infty} \delta^4(sk_1 + q_1 - q_2 - k_2)\; A_{s\lambda_1\lambda_2\lambda_3\lambda_4} \ , \tag{2.11}$$

where

$$A_{s\lambda_1\lambda_2\lambda_3\lambda_4} = B_s\, A_{0s\lambda_1\lambda_2\lambda_3\lambda_4} + B_{1s}\, A_{1s\lambda_1\lambda_2\lambda_3\lambda_4} + B_{2s}\, A_{2s\lambda_1\lambda_2\lambda_3\lambda_4} \ , \tag{2.12}$$

$$B_s = J_s(z) \ ,$$

$$B_{1s} = -\frac{1}{2}\,[J_{s-1}(z) + J_{s+1}(z)] \ ,$$

$$B_{2s} = \frac{1}{2i}\,[J_{s-1}(z) - J_{s+1}(z)] \ ,$$

J_s is a Bessel function of the first kind,

$$z = \frac{\xi m \sin\theta}{e + px}\,(s-\eta) \ ,$$

$$A_{0s\lambda_1\lambda_2\lambda_3\lambda_4} = \bar{u}(p_2\lambda_3)\left[\not{e}^*_{\lambda_2} + \frac{\xi^2 m^2}{2}\frac{(k_1\cdot e^*_{\lambda_2})}{(k_1\cdot p_1)(k_1\cdot p_2)}\not{k}_1\right] u(p_1\lambda_4) \ ,$$

$$A_{1s\lambda_1\lambda_2\lambda_3\lambda_4} = \bar{u}(p_2\lambda_3)\,\frac{\xi m}{2}\left[\frac{1}{k_1\cdot p_2}\gamma_x \not{k}_1 \not{\epsilon}^*_{\lambda_2} + \frac{1}{k_1\cdot p_1}\not{\epsilon}^*_{\lambda_2}\not{k}_1\gamma_x\right] u(p_1\lambda_4)\ ,$$

$$A_{2s\lambda_1\lambda_2\lambda_3\lambda_4} = \bar{u}(p_2\lambda_3)\,\frac{\xi m}{2}\left[-\frac{1}{k_1\cdot p_2}\gamma_y \not{k}_1 \not{\epsilon}^*_{\lambda_2} - \frac{1}{k_1\cdot p_1}\not{\epsilon}^*_{\lambda_2}\not{k}_1\gamma_y\right] u(p_1\lambda_4)\ .$$

Notice that we have chosen $\lambda_1 = (-1)$ because cases involving $\lambda_1 = +1$ can be obtained by mirror imaging, which reverses the helicities of all particles. Here, $e^*_{\lambda_2}$ is the complex conjugate of the polarization vector for the outgoing photon.

For λ_2 = positive,

$$e^*_{\lambda_2} = \left(0\ ,\ \frac{\cos\theta}{\sqrt{2}}\ ,\ \frac{-i}{\sqrt{2}}\ ,\ \frac{-\sin\theta}{\sqrt{2}}\right)\ .$$

For λ_2 = negative,

$$e^*_{\lambda_2} = \left(0, \frac{\cos\theta}{\sqrt{2}}\ ,\ \frac{+i}{\sqrt{2}}\ ,\ \frac{-\sin\theta}{\sqrt{2}}\right)\ .$$

We notice A_0, A_1, A_2 are independent of s because only k_1 is dependent on s and k_1 appears in both the numerator and denominator with equal power. The explicit representations of spinors are given in Appendix B.

After obtaining the helicity amplitudes $A_{s\lambda_1\lambda_2\lambda_3\lambda_4}$ as shown in (2.12), we can sum over the helicities of the outgoing electron λ_3 and obtain

$$W_{s\lambda_1\lambda_2\lambda_4} = A^2_{s\lambda_1\lambda_2 p\lambda_4} + A^2_{s\lambda_1\lambda_2 n\lambda_4}\ . \tag{2.13}$$

There are altogether eight $W_{s\lambda_1\lambda_2\lambda_3}$'s, but only four of them are independent because of parity conservation,

$$W_{snnn} = W_{sppp}\ ,$$

$$W_{snnp} = W_{sppn}\ ,$$

$$W_{snpn} = W_{spnp} ,$$

$$W_{snpp} = W_{spnn} .$$

Suppose there are in total N events which are induced by four possible combinations of initial helicities $N_{\lambda_1\lambda_4}$.

$$N = N_{pp} + N_{nn} + N_{np} + N_{pn}.$$

The number of events with λ_2 = positive is

$$N_p = N_{pp}\sum_s W_{sppp} + N_{pn}\sum_s W_{sppn} + N_{np}\sum_s W_{snpp} + N_{nn}\sum_s W_{snpn} .$$

The number of events with λ_2 = negative is

$$N_n = N_{pp}\sum_s W_{spnp} + N_{pn}\sum_s W_{spnn} + N_{np}\sum_s W_{snnp} + N_{nn}\sum_s W_{snnn}.$$

Let $P(k_2)$ be the polarization of k_2. By definition

$$P(k_2) = \frac{N_p - N_n}{N_p + N_n} = \frac{(N_{pp} - N_{nn})\sum_s D_{spp} + (N_{pn} - N_{np})\sum_s D_{spn}}{(N_{pp} + N_{nn})\sum_s S_{spp} + (N_{pn} + N_{np})\sum_s S_{spn}} , \quad (2.14)$$

where

$$D_{spp} \equiv W_{sppp} - W_{spnp} ,$$

$$S_{spp} \equiv W_{sppp} + W_{spnp} ,$$

$$D_{spn} \equiv W_{sppn} - W_{spnn} ,$$

$$S_{spn} \equiv W_{sppn} + W_{spnn} .$$

Now the polarization of k_1 is defined by

$$P(k_1) = \frac{N_{pn} - N_{nn}}{N_{pn} + N_{nn}} = \frac{N_{pp} - N_{np}}{N_{pp} + N_{np}} , \quad (2.15)$$

and the polarization of p_1 is defined by

$$P(p_1) \;=\; \frac{N_{pp}-N_{pn}}{N_{pp}+N_{pn}} = \frac{N_{np}-N_{nn}}{N_{np}+N_{nn}} \;. \tag{2.16}$$

From (2.14)–(2.16), we obtain finally

$$P(k_2) \;=\; \frac{P(k_1)\sum_s N_{1s} + P(p_1)\sum_s N_{2s}}{\sum_s D_{1s} + P(k_1)P(p_1)\sum_s D_{2s}} \;, \tag{2.17}$$

where

$$N_{1s} \;=\; (D_{spp}+D_{spn})/m^2 \;, \qquad N_{2s} \;=\; (D_{spp}-D_{spn})/m^2 \;,$$

$$D_{1s} \;=\; (S_{spp}+S_{spn})/m^2 \;, \qquad D_{2s} \;=\; (S_{spp}-S_{spn})/m^2 \;.$$

We let the MAPLE grind through all the above computations and obtain the expressions for N_{1s}, N_{2s}, D_{1s}, and D_{2s} as follows:

$$\begin{aligned} N_{1s} \;=\; & \{[-(6+2x)y^3-(2-2x)y]\,\xi^2+4y^5-4y^3\}\,\frac{\xi\sin\theta}{d_1}J_s(J_{s-1}-J_{s+1}) \\ & +\{(1+6x+x^2)y^4-(1-2x+x^2)\}\,\frac{\xi^2}{d_1}\,[J_{s-1}^2-J_{s+1}^2] \;, \end{aligned} \tag{2.18}$$

$$\begin{aligned} N_{2s} \;=\; & \{-(4-4x^2)(y^4-y^2)\,\xi^2+(2-2x^2)y^6-(2+4x-6x^2)y^4 \\ & -(2-8x+6x^2)y^2+(2-4x+2x^2)\}\,\frac{1}{d_1}\,J_s^2+\{(2-2x)(y^3-y)\,\xi^2 \\ & +4xy^5-4xy^3\}\,\frac{\xi\sin\theta}{d_1}\,J_s(J_{s-1}+J_{s+1}) \\ & -(4-4x^2)(y^4-y^2)\,\frac{\xi^2}{d_1}\,J_{s-1}J_{s+1} \\ & +(1-2x+x^2)(y^4-1)\,\frac{\xi^2}{d_1}\,(J_{s-1}^2+J_{s+1}^2) \;, \end{aligned} \tag{2.19}$$

$$\begin{aligned} D_{1s} \;=\; & -8J_s^2+\frac{\xi^2}{d_1}\,[(5+2x+x^2)y^4+(2-2x^2)y^2 \\ & +(1-2x+x^2)]\,[J_{s-1}^2+J_{s+1}^2-2J_s^2] \;, \end{aligned} \tag{2.20}$$

$$D_{2s} = \{[-(2-2x)(y^3-y)]\,\xi^2 + 4(y^5-y^3)\}\,J_s(J_{s-1}-J_{s+1})\,\frac{\xi\sin\theta}{d_1}$$
$$-(1-x)^2(y^4-1)\,\frac{\xi^2}{d_1}\,(J_{s-1}^2 - J_{s+1}^2)\,, \qquad (2.21)$$

where $d_1 = y^2[y^2(1+x)+(1-x)]$, $x = \cos\theta$, and $y = (e+p)/m$, x and y will be given in terms of laboratory quantities later in Eqs. (2.36) and (2.37).

The lowest order Compton case for Eq. (2.17) can be obtained by letting $s = 1$, $J_s = \xi y \sin\theta[y^2(1+x)+(1-x)]^{-1}$, $J_{s-1} = 1$, $J_{s+1} = 0$, and retaining only ξ^2 terms in N_{1s}, N_{2s}, D_{1s} and D_{2s}. The result can be written

$$N_1 = \xi^2[y^2(1+x)-1+x]$$
$$\times[y^4(x^2+2x+5)+2y^2(1-x^2)+(1-x)^2]\,y^2/d_1^2\,, \qquad (2.22)$$

$$N_2 = \xi^2(1-x)\,[y^6(x^2+4x+3)+y^4(x^2-6x-3)$$
$$-(x^2-1)\,y^2-(1-x)^2]\,y^2/d_1^2\,, \qquad (2.23)$$

$$D_1 = \xi^2[y^6(x^3+3x^2+7x+5)-y^4(3x^3-5x^2+x+1)$$
$$+y^2(3x^3-3x^2-3x+3)-(x^3-3x^2+3x-1)]\,y^2/d_1^2\,, \qquad (2.24)$$

$$D_2 = \xi^2[y^2(1+x)-1+x]$$
$$\times[y^4(-x^2-2x+3)+y^2(2x^2-2)-(1-x)^2]\,y^2/d_1^2\,. \qquad (2.25)$$

The differential cross section for the process $sk_1 + q_1 \rightarrow k_2 + q_2$ is proportional to D_{1s}.

$$d\sigma_s = \frac{1}{4k_1\cdot q_1}\,\frac{1}{(2\pi)^2}\,\frac{d^3k_2}{2w_2}\,\frac{d^3q_2}{2q_{20}}\,\delta^4(sk_1+q_1-k_2-q_2)\,\left[(\alpha 4\pi)^2\,\frac{D_{1s}}{\xi^2}\right]\,, \qquad (2.26)$$

which can be simplified into

$$\frac{d\sigma_s}{du} = \frac{\pi\alpha^2}{4w_1E_1\xi^2}\,D_{1s}\,, \qquad (2.27)$$

where w_1 and E_1 are laboratory incident photon and electron energies respectively and $u = w_2/E_1$.

Terms in the square bracket in Eq. (2.26) can be understood in the following way: $(\alpha 4\pi)^2 = e^4$ comes from incoming and outgoing photons coupled to the electron. The $m^2\xi^2$ in the denominator is equal to $4\pi\alpha a^2$, which is put there so that in the limit $\xi \to 0$ and $s = 1$, $d\sigma_s$ gives the Compton cross section. This factor is evident by inspecting the definition of $\vec{A}$ given by Eq. (2.10). We also notice that in Eq. (2.26) the flux density is given by $4k_1 \cdot q_1$, not by $4sk_1 \cdot q_1$. Conceptually this is because the number of photons acting coherently is not *a priori* given by the laser beam but is determined by the matrix elements of the interaction. The differential cross section is obtained by the sum with respect to all s:

$$\frac{d\sigma}{du} = \sum_{s=1}^{\infty} \frac{d\sigma_s}{du} = \frac{\pi\alpha^2}{4w_1E_1\xi^2} \sum_{s=1}^{\infty} D_{1s} \,. \tag{2.28}$$

Assuming that the size of the electron beam is much smaller than that of the laser beam, the number of events per incident electron within an infinitesimal length dl (cm) of the laser beam is

$$\frac{d^2W}{du} = n_\gamma \, dl \, \frac{d\sigma}{du} \,, \tag{2.29}$$

where n_γ is number of laser photons per cm^3 given by Eq. (A1).

Thus, the total number of scattered photons per incident electron in dl is [5]

$$\begin{aligned} dW &= \int_{u_{\min}}^{u_{\max}} du \, n_\gamma \, dl \sum_{s=1}^{\infty} \frac{d\sigma_s}{du} \\ &= \frac{\alpha dl m^2}{16E_1} \sum_{s=1}^{\infty} \int_{u_{\min}}^{u_{\max}} du \left(\frac{1}{197 \times 10^{-13} \text{ cm MeV}}\right) D_{1s} \end{aligned}$$

$$= 6.024 \times 10^3 \frac{dl\ (\mathrm{cm})}{E_1\ (\mathrm{GeV})} \sum_{s=1}^{\infty} \int_{u_{\min}}^{u_{\max}} D_{1s}\, du\ . \qquad (2.30)$$

Now we see why we have to use the infinitesimal length dl instead of the total pulse length L of the laser beam. We know that W cannot exceed 1, when u is near 1 because of energy conservation. For our purpose, it is a good approximation to assume that an electron once it is scattered by the laser photon will be lost as a scatterer to produce high energy photon. This assumption is justified by the shape of D_{1s}, which has a more prominent peak at the high value of u than at the low value of u. If this approximation is made, we can use the total cross section σ as the coefficient of attenuation. We then have

$$dW = n_\gamma\ \exp\{-n_\gamma \sigma l\}\ dl\ \frac{d\sigma}{du}\ .$$

Integrating the above with respect to l and u, we obtain the number of scattered photons per incident electron:

$$W = (1 - \exp\{-n_\gamma \sigma L\})\ \frac{1}{\sigma} \int_{u_{\min}}^{u_{\max}} du\ \sum_{s=1}^{\infty}\ \frac{d\sigma_s}{du}\ . \qquad (2.31)$$

This equation is applicable when both $u_{\min}$ and $u_{\max}$ are not much smaller than 1. On the other hand, when u is much less than 1, an electron can scatter with the incoming laser photons many times before losing a substantial fraction of its energy. In this case there can be more than one back-scattered photon per incident electron, and thus W can be greater than 1. This happens, for example, when $E_1 = 1$ GeV and $\omega_1 = 1$ eV, and thus $u_{\max} = 0.016$ for $\xi \to 0$ and $s = 1$. When the multiple scattering is important, we need to consider the straggling instead of the attenuation. The problem of straggling can be handled by the Monte Carlo method numerically.

The numerical evaluations of N_{1s}, N_{2s}, D_{1s}, and D_{2s} are performed in the following way: we first specify the values of incident laser photon energy (ω_1) and incident electron energy (E_1), and laser intensity (ξ). Since this is a two-body problem, the laboratory angle θ_l (which is the angle bwtween $\vec{k}_2$ and $\vec{p}_1$) is related to the laboratory scattered photon energy $\omega_2 \equiv E_1 u$ by

$$\theta_l = \frac{1}{\gamma_1}\sqrt{w\left(\frac{1}{u}-1\right)-(1+\xi^2)}\,, \tag{2.32}$$

where $\gamma_1 = E_1/m$, $w = 4sE_1\omega_1/m^2$, or

$$u \equiv \frac{\omega_2}{E_1} = \frac{1}{1+(1+\xi^2+\gamma_1^2\theta_l^2)/w}\,, \tag{2.33}$$

from which we obtain $u_{\min} = 0$ and

$$u_{\max} = \frac{1}{1+(1+\xi^2)/w}\,. \tag{2.34}$$

The argument for the Bessel function is

$$z = \frac{\xi m\theta_l}{2\omega_1(1/u-1)}\,. \tag{2.35}$$

Then y and x appearing in N_{1s}, N_{2s}, D_{1s}, and D_{2s} can be written in terms of laboratory quantities as

$$y \equiv \frac{e+p}{m} = \left[1+w-\xi^2\,\frac{u}{1-u}\right]^{1/2}\,, \tag{2.36}$$

$$x \equiv \cos\theta = -\left(1-\frac{\omega_2^2\theta_l^2}{p^2}\right)^{1/2}\ \text{sign}\,, \tag{2.37}$$

where sign $= [u-0.5\,(1-y^{-2})]/\,|u-0.5\,(1-y^{-2})|$, and $p = m(y^2-1)/2y$.

For convenience of discussion we have specified E_1, ω_1, u, and ξ as input variables for evaluating D_{1s}, D_{2s}, N_{1s}, and N_{2s}. However, these functions depends only on center-of- mass energies w, u, and ξ. In other words,

these functions depend only the product $E_1\omega_1$, but not E_1 and ω_1 separately. Here $u_{\max}$ depends only on w and ξ, as seen from Eq. (2.34). Thus, as long as $u_{\max}$ and ξ are given, the functions D_{1s}, D_{2s}, N_{1s}, and N_{2s} are specified.

From the definitions of N_{1s}, N_{2s}, D_{1s}, and D_{2s} given in Eq. (2.17), we obtain

$$\begin{aligned} A &= \frac{\sum_s N_{1s}}{\sum_s D_{1s}} \\ &= \frac{d\sigma(\lambda_1=\lambda_2) - d\sigma(\lambda_1=-\lambda_2)}{d\sigma(\lambda_1=\lambda_2) + d\sigma(\lambda_1=-\lambda_2)} , \end{aligned} \tag{2.38}$$

$$\begin{aligned} B &= \frac{\sum_s N_{2s}}{\sum_s D_{1s}} \\ &= \frac{d\sigma(\lambda_4=\lambda_2) - d\sigma(\lambda_4=-\lambda_2)}{d\sigma(\lambda_4=\lambda_2) + d\sigma(\lambda_4=-\lambda_2)} , \end{aligned} \tag{2.39}$$

$$\begin{aligned} C &= \frac{\sum_s D_{2s}}{\sum_s D_{1s}} \\ &= \frac{d\sigma(\lambda_1=\lambda_4) - d\sigma(\lambda_1=-\lambda_4)}{d\sigma(\lambda_1=\lambda_4) + d\sigma(\lambda_1=-\lambda_4)} , \end{aligned} \tag{2.40}$$

where, for example, $d\sigma(\lambda_1=\lambda_2)$ means the differential cross section $(d\sigma/du)$ in which λ_3 and λ_4 are summed and λ_1 and λ_2 are set either both positive or both negative. From the parity conservation, the two possibilities have equal probability. These relations tell us that A, B, and C are not just the coefficients of $P(k_1)$, $P(p_1)$, and $P(k_1)\,P(p_1)$ in the definition of $P(k_2)$,

$$P(k_2) = \frac{P(k_1)\,A + P(p_1)\,B}{1 + P(k_1)\,P(p_1)\,C} , \tag{2.41}$$

but also that they have definite physical meanings. In fact, the quantity C defined in Eq. (2.40) plays a very crucial role in the measurement of helicity of electrons using the polarized laser photon beams shown in the following.

Measurement of Helicity of $e^{\pm}$ using circularly polarized laser beams

At SLAC the helicity of the electron beam is measured in two ways: one by the Møller scattering on the polarized atomic electron target and the other by the Compton scattering on the circularly polarized laser beam. Here we describe the latter. Let the number of events induced by the positive ($\lambda_1 = p$) and negative ($\lambda_1 = n$) helicity laser beam be $N(p)$ and $N(n)$ respectively. We have

$$\begin{aligned} N(p) &= N_{pp}\left(\sum_s W_{spnp} + \sum_s W_{sppp}\right) \\ &+ N_{pn}\left(\sum_s W_{sppn} + \sum_s W_{spnn}\right) , \end{aligned} \tag{2.42}$$

$$\begin{aligned} N(n) &= N_{np}\left(\sum_s W_{snnp} + \sum_s W_{snpp}\right) \\ &+ N_{nn}\left(\sum_s W_{snpn} + \sum_s W_{snnn}\right) . \end{aligned} \tag{2.43}$$

Then the asymmetry can be written

$$A_{\rm sym} \equiv \frac{N(p) - N(n)}{N(p) + N(n)} = \frac{P(k_1) + P(p_1)\,C}{1 + P(k_1)P(p_1)\,C} \longrightarrow P(p_1)\,C\ . \tag{2.44}$$

If we let the number of positive helicity photons used to measure $N(p)$ be equal to that used to measure $N(n)$, then $P(k_1)$ becomes zero, and the last expression results. Since C as given by Eq. (2.40) is a calculable function, we can obtain the polarization of the electron $P(p_1)$ by measuring $A_{\rm sym}$. This technique is well known. Our contribution here is to include the effects due to contributions from $s \geq 2$. In the measurement of the polarization using the asymmetry, the energy of the outgoing electron E_2 is measured. Since $E_2 = E_1(1-u)$, we can see the E_2 dependence of $A_{\rm sym}$ from graphs shown in Figs. 3 and 6 through 9. The most interesting features of these curves are

that D_{2s} and N_{1s} have zeros at the same value of u, which corresponds to the photon scattering angle of 90° in the rest frame of the initial electron, given by

$$u_o = \frac{1-(1+\frac{1}{2}w+\frac{1}{2}\xi^2)^{-1}}{1+\frac{\xi^2}{w}}, \tag{2.45}$$

where $w = (4sw_1E_1)/m^2$. The value of u_0 increases as s is increased, but it decreases as ξ is increased. When ξ is large and the $s \geq 2$ contribution becomes important, the zero in the $s = 1$ contribution becomes partially filled. We also notice that in the Thomson limit, $w \to 0$, we have $D_{2s} = 0$, and thus the method cannot be used in this limit.

There must be a simple reason why these zeros occur for N_{1s} and D_{2s}, but not for N_{2s}. At this moment, this author is unable to find a simple explanation.

Observations:

1. From the expression of $u_{\max}$ given by Eq. (2.34), we see that if the center-of-mass energy is much greater than the effective mass m^*, then $u_{\max}$ approaches unity. On the other hand, if $4E_1\omega_1 s \ll m^2(1+\xi^2)$, we have $u_{\max} \to 0$. If $4E_1\omega_1 \gg m^2(1+\xi^2)$, then $u_{\max}$ approaches unity for all s. On the other hand, $u_{\max}$ changes greatly for different s's when the center-of-mass energy is comparable to or less than m^*. In the latter case, the modes with $s \geq 2$ spoil both the energy distribution and the quality of polarization of the scattered photon beam. Thus ξ should be chosen much less than 1, but the laser pulse length should be increased to obtain high luminosity. See Eq. (2.31).

2. The σ_s is roughly proportional to ξ^{2s}. Thus when ξ^2 is much less than unity, only σ_1 survives, and it reduces to the Compton scattering cross section. In the Compton limit (i.e., $\xi^2 \to 0$) we may write the polarization of the scattering photon [see Eq. (2.17)]

$$P(k_2) = \frac{P(k_1)A + P(p_1)B}{1 + P(k_1)\,P(p_1)C}\ , \tag{2.46}$$

with $A = N_1/D_1$, $B = N_2/D_1$, and $C = D_2/D_1$, where N_1, N_2, D_1, and D_2 are given respectively by Eqs. (2.22–2.25). In Fig. (3) we show A, B, and C in Eq. (2.38) for three sets of energies: (a) $\omega_1 = 3.5$ eV and $E_1 = 1$ GeV, (b) $\omega_1 = 1.17$ eV, and $E_1 = 50$ GeV, and (c) $\omega_1 = 3.5$ eV and $E_1 = 500$ GeV. The values of $u_{\max}$ for each case indicate how relativistic the reaction is in the center-of-mass system. (a) is the low-energy case and almost the Thomson limit, which is characterized by D_1 being symmetric with respect to $u = u_{\max}/2$ and$A$ being antisymmetric with respect to $u = u_{\max}/2$ and $B = C = 0$. In the Thomson limit, the polarization of k_2 is opposite to that of k_1 at the high-energy end, but at the low-energy end it is the other way. The polarization of the incident electron does not contribute to the polarization of k_2 in the Thomson limit because $B \to 0$. As the center-of-mass energy is increased, the energy distribution (i.e., D_1) gets skewed toward the high-energy end and B becomes more prominent and A becomes less so. This means that at high center-of-mass energy the polarization of k_2 is dominated by the polarization of the incident electron (p_1).

Figure 4 illustrates that at an intermediate center-of-mass energy ($W_1 = 1.17$ eV, $E_1 = 50$ GeV), if the incident electron (p_1) and the laser

photon (k_1) are polarized, it somewhat improves the polarization of the outgoing photon (k_2).

Figure 5 illustrates the effect of high ξ. The energy is the same as in Fig. 3(a); i.e., almost the Thomson limit. For simplicity we consider that only the laser beam is polarized, so that the polarization of k_2 is

$$P(k_2) \;=\; P(k_1)\,\sum_{s=1}^{\infty} N_{1s} \Big/ \sum_{s=1}^{\infty} D_{1s}\;. \tag{2.47}$$

The denominator of the Eq. (2.39) gives the energy distribution—D_{1s} for $s = 1, 2$, and 3 are displayed in Fig. 5(a), and N_{1s} is displayed in Fig. 5(b) for $\xi = 1$. We first notice that higher s contributions to the numerator and the denominator tend to spoil the characteristics of polarization and the energy distribution respectively. We conclude that a high value of ξ is not desirable at low center-of-mass energy.

In Figs. 6–9 we present graphs for N_{1s}, N_{2s}, and D_{1s}, D_{2s}, defined by Eqs. (2.18)–(2.21) for two set of energies, two values of ξ and three values of s. The most interesting characteristics of cases with $s \geq 2$ is that at $u = u_{\max}$ and $u = 0$, all these functions are zero, whereas for $s = 1$ these function have maximum at $u = u_{\max}$. This is because the Bessel function at the origin is nonzero only for $J_0(0) \neq 0$, which can happen only when $s = 1$ for $J_{s-1}(0)$.

Thomson and Pseudo–Thomson limit

Let us denote the limits $\xi \to 0$ and $w \equiv 4w_1\,E_1/m^2 \to 0$ as the Thomson limit, and $w \to 0$ but ξ is not small as the Pseudo–Thomson limit. For example, scattering of a laser beam by an electron beam of less than 100 MeV belongs to the Pseudo–Thomson limit. In the Pseudo–Thomson

limit we have

$$z = \frac{2s\xi}{\sqrt{1+\xi^2}} \frac{\gamma_* \theta_l}{1+\gamma_*^2\theta_l^2} , \tag{2.48}$$

$$\gamma_* = \frac{E_1/m}{\sqrt{1+\xi^2}} , \tag{2.49}$$

$$y^2 = 1 + w - \xi^2 u , \tag{2.50}$$

$$x = -\frac{1-\gamma_1^2\theta_l^2}{1+\gamma_1^2\theta_l^2} , \tag{2.51}$$

$$\gamma_1^2\theta_l^2 = w\left(\frac{1}{u} - \frac{1}{u_{\max}}\right) , \tag{2.52}$$

$$N_{1s} = \left[-4\xi^3 \sin\theta + \left(\frac{8s}{z}\right) x\, \xi^2\right] J_s \left(J_{s-1} - J_{s+1}\right) , \tag{2.53}$$

$$N_{2s} = 0 ,$$

$$D_{1s} = -8J_s^2 + 4\xi^2 \left[J_{s-1}^2 + J_{s+1}^2 - 2J_s^2\right] , \tag{2.54}$$

$$D_{2s} = 0 .$$

When $\gamma_*\theta_l \ll 1$, we have $z \to 0$ and thus only $s = 1$ is important, and furthermore $J_s = z/2$, $J_{s-1} = 1$, and $J_{s+1} = 0$. In this limit, we have

$$N_{11} = 4\xi^2 x , \tag{2.55}$$

$$D_{11} = 2\xi^2 \left(1 + x^2\right) . \tag{2.56}$$

The polarization of k_2 is thus independent of the polarization of p_1 and

$$P(k_2) = \frac{2x}{1+x^2} P(k_1) . \tag{2.57}$$

The energy and angle of k_2 are related by

$$\frac{u}{u_{\max}} = \frac{1}{1+\gamma_*^2\theta_l^2} , \tag{2.58}$$

with $u_{\max} = 4w_1E_1/m_*^2$.

The differential cross section is

$$\frac{d\sigma}{du} = \frac{2\pi r_0^2}{w}(1+x^2) . \tag{2.59}$$

The Thomson limit is obtained by setting $\xi = 0$ in Eqs. (2.57) and (2.59).

We have used the rest frame of $(p_2 + k_2)$ to obtain the relatively compact expressions for $N_{1s}, N_{2s}, D_{1s}, D_{2s}$ as shown in Eqs. (2.18) through (2.21). The simplification occurs because in this frame the complicated expression $(s - \eta)$ occurs only in the definition of k_1 as shown in Eq. (2.6) and k_1 appears with equal power in the numerators and the denominators of A_0, A_1, A_2 defined by Eq.(2.12). Thus A_0, A_1, A_2 do not contain the factor $(s - \eta)$ in this frame. In the Compton limit $s - \eta = 1$, so we do not have to resort to this frame. Actually we can obtain simpler expressions for N_1, N_2, D_1, D_2 in the rest system of the initial electron $p_1 = (m, 0, 0, 0)$. In Appendix C we give expressions for N_1, N_2, D_1, D_2 in the rest system of the initial electron and also in terms of the variables $u = \omega_2/E_1$ and $w = 4\omega_1 E_1/m^2$.

3. Laser (k_1)+ high energy photon $(k_2) \to e^+ + e^-$.

Our purpose here is to investigate the properties of e^+ or e^-, including their polarization when both k_1 and k_2 are circularly polarized. The initial state can have an even or odd number of photons in the reaction $sk_1 + k_2 \to p_1 + p_2$. Since amplitudes for different s's do not interfere, the

final state has a definite charge parity for a given s; thus one cannot distinguish e^- from e^+ in this problem. However, we shall call p_1 positron and p_2 electron for convenience in applying the substitution rule to the previous problem. The Feynman diagrams for the present problem (Fig. 10) and the previous problem (Fig. 1) are related by the substitution rule: $k_2 \to -k_2$, $p_1 \to -p_1$, $u(p_1) \to v(-p_1)$, and $\epsilon_2^* \to \epsilon_2$.

Let us denote the helicity amplitude in the laboratory system by $T_{s\lambda_1\lambda_2\lambda_3\lambda_4}$ for the reaction $sk_1 + k_2 \to e^+ + e^-$, where λ_1, λ_2, λ_3 and λ_4 are laboratory helicities of k_1 (laser), k_2 (high energy γ), p_2 (electron) and p_1 (positron) respectively. Again out of 16 helicity amplitudes, only 8 are independent because of the parity conservation, which results in $T_{s\lambda_1\lambda_2\lambda_3\lambda_4} = T_{s,-\lambda_1,-\lambda_2,-\lambda_3,-\lambda_4}$.

The matrix element for laser photon plus high-energy $\gamma \to e^+e^-$ can be written

$$(S_{fi})_{\lambda_1\lambda_2\lambda_3\lambda_4} = \frac{-ie}{\sqrt{8q_{10}q_{20}\omega_2}}(2\pi)^4 \sum_{s=1}^{\infty} \delta^4(sk_1+k_2-q_1-q_2)\, T_{s\lambda_1\lambda_2\lambda_3\lambda_4} \ , \quad (3.1)$$

where q_{10}, q_{20} and ω_2 are all laboratory energies of q_1, q_2 and k_2 respectively.

The helicity amplitude $T_{s\lambda_1\lambda_2\lambda_3\lambda_4}$ can be written as

$$T_{s\lambda_1\lambda_2\lambda_3\lambda_4} = B_s T_{0s\lambda_1\lambda_2\lambda_3\lambda_4} + B_{1s} T_{1s\lambda_1\lambda_2\lambda_3\lambda_4} + B_{2s}\, T_{2s\lambda_1\lambda_2\lambda_3\lambda_4} \ , \quad (3.2)$$

where B_s, B_{1s}, and B_{2s} are the same as those defined in Eq. (2.12). The argument of Bessel functions z is now

$$z = \frac{\xi m \theta_1}{2\omega_1(1-u)} \ , \quad (3.3)$$

where θ_1 is the laboratory angle between $\vec{p}_1$ and $\vec{k}_2$ (see Fig. 11), ω_1 is the energy of the laser photon, and $u = E_1/\omega_2$ with E_1 and ω_2 being the energy

of the outgoing positron and the incident high energy γ respectively, and θ_1 is related to u by

$$\theta_1 = \frac{1}{u\omega_2} \left[4s\omega_1\omega_2 u(1-u) - m^2(1+\xi^2)\right]^{1/2} , \tag{3.4}$$

and ξ is the parameter defined in Appendix A.

$$T_{0s\lambda_1\lambda_2\lambda_3\lambda_4} = \bar{u}(p_2,\lambda_3)\not{e}_{\lambda_2} v(-p_1,\lambda_4) , \tag{3.5}$$

$$T_{1s\lambda_1\lambda_2\lambda_3\lambda_4} = \bar{u}(p_2,\lambda_3)\,\frac{\xi m}{2}\left[\frac{1}{k_1\cdot p_2}\gamma_x \not{k}_1 \not{e}_{\lambda_2} + \frac{1}{k_1\cdot p_1}\not{e}_{\lambda_2}\not{k}_1\gamma_x\right] v(-p_1,\lambda_4) , \tag{3.6}$$

$$T_{2s\lambda_1\lambda_2\lambda_3\lambda_4} = \bar{u}(p_2,\lambda_3)\,\frac{\xi m}{2}\left[\frac{1}{k_1\cdot p_2}\gamma_y \not{k}_1 \not{e}_{\lambda_2} + \frac{1}{k_1\cdot p_1}\not{e}_{\lambda_2}\not{k}_1\gamma_y\right] v(-p_1,\lambda_4) . \tag{3.7}$$

Here, e_{λ_2} is the polarization vector for the high energy incident photon k_2: for λ_2 = positive,

$$e_{\lambda_2} = (0\,,\frac{1}{\sqrt{2}}\,,\frac{i}{\sqrt{2}}\,,0) ; \tag{3.8}$$

for λ_2 = negative,

$$e_{\lambda_2} = (0\,,\frac{1}{\sqrt{2}}\,,\frac{-i}{\sqrt{2}}\,,0) . \tag{3.9}$$

$$q_1 = p_1 + \frac{\xi^2 m^2}{2p_1\cdot k_1}\, k_1 . \tag{3.10}$$

$$q_2 = p_2 + \frac{\xi^2 m^2}{2p_2\cdot k_1}\, k_1 . \tag{3.11}$$

The explicit representations of spinors are given in Appendix B. Using the notations of (B.1) through (B.4), we have

$$u(p_2,\pm) = u(p_2,\theta_2,\pi,\pm.5) , \tag{3.12}$$

$$v(-p_1, \pm) = v(p_1, \theta_1, 0, \pm .5) \ . \tag{3.13}$$

The p_2, θ_2, p_1, and θ_1 can all be written as functions of u, ω_1, ω_2, and ξ. Equation (3.4) gives θ_1.

Assuming $\omega_2 \gg \omega_1$, $E_1 \gg m$, $E_2 \gg m$, $\theta_2 \ll 1$, and $\theta_1 \ll 1$, we have:

$$E_1 = \omega_2 u \ , \tag{3.14}$$

$$E_2 = \omega_2 (1 - u) \ , \tag{3.15}$$

$$\theta_2 = \theta_1 E_1 / E_2 \ . \tag{3.16}$$

Using exactly the same argument as in Sec. 2, we obtain the differential cross section and the polarization for the positron (also applicable to the electron because of charge symmetry).

From the helicity amplitudes, we obtain the differential cross section and the polarization for the positron (also applicable to the electron because of charge symmetry) in terms of N_{1s}, N_{2s}, D_{1s}, and D_{2s} defined as follows:

$$N_{1s} = \frac{1}{2m^2} \sum\nolimits_{\lambda_1 \lambda_3} (T^2_{sn\lambda_2\lambda_3 n} + T^2_{sp\lambda_2\lambda_3 p} - T^2_{sn\lambda_2\lambda_3 p} - T^2_{sp\lambda_2\lambda_3 n}) \tag{3.17}$$

$$N_{2s} = \frac{1}{2m^2} \sum\nolimits_{\lambda_1 \lambda_3} (T^2_{s\lambda_1 n\lambda_3 n} + T^2_{s\lambda_1 p\lambda_3 p} - T^2_{s\lambda_1 p\lambda_3 n} - T^2_{s\lambda_1 n\lambda_3 p}) \ , \tag{3.18}$$

$$D_{1s} = \frac{1}{2m^2} \sum\nolimits_{\lambda_1 \lambda_2 \lambda_3 \lambda_4} T^2_{s\lambda_1\lambda_2\lambda_3\lambda_4} \ , \tag{3.19}$$

$$D_{2s} = \frac{1}{2m^2} \sum\nolimits_{\lambda_3 \lambda_4} (T^2_{snn\lambda_3\lambda_4} + T^2_{spp\lambda_3\lambda_4} - T^2_{snp\lambda_3\lambda_4} - T^2_{spn\lambda_3\lambda_4}) \ , \tag{3.20}$$

where n and p refer to negative and positive helicities respectively.

The differential cross section for each s is

$$d\sigma_s = \frac{1}{8\omega_1\omega_2} \frac{1}{(2\pi)^2} \frac{d^3q_1}{2q_{10}} \delta\left[(sk_1 + k_2 - q_1)^2 - m_*^2\right] \left[(\alpha 4\pi)^2 \frac{D_{1s}}{\xi^2}\right] \ , \tag{3.21}$$

which can be simplified to

$$\frac{d\sigma_s}{du} = \frac{\pi\alpha^2}{4\omega_1\omega_2\xi^2}\, D_{1s}\ . \tag{3.22}$$

The total cross section is

$$\sigma \;=\; \sum_{s=1}^{\infty}\sigma_s \;=\; \frac{\pi\alpha^2}{4\omega_1\omega_2\xi^2}\ \sum_{s=1}^{\infty}\ \int_{u_{\min}}^{u_{\max}}\ D_{1s}\ du\ ,$$

where $u_{\max}$ and $u_{\min}$ are given by Eq. (3.30).

The polarization of e^+ (or e^-) is

$$P(p_1) \;=\; P(p_2) \;=\; \frac{P(k_1)\sum_s N_{1s} + P(k_2)\sum_s N_{2s}}{\sum_s D_{1s} + P(k_1)P(k_2)\sum_s D_{2s}}\ . \tag{3.23}$$

We notice that in D_{1s} and D_{2s}, the spins of both the electron (λ_4) and positron (λ_3) are summed, and hence they can be calculated in any frame. We have calculated these two quantities in both the center-of-mass and the laboratory system. The numerical results agree completely. In the center-of-mass system, simple analytical expressions for D_{1s} and D_{2s} can be obtained:

$$D_{1s} = J_s^2 4 + 2\xi^2 \frac{(e^2+p^2x^2)}{e^2-p^2x^2} (J_{s-1}^2 + J_{s+1}^2 - 2J_s^2) . \tag{3.24}$$

$$\begin{aligned} D_{2s} &= -J_s(J_{s-1} - J_{s+1}) \frac{2zm^{-2}}{s-\eta} (e^2+p^2x^2) \\ &\quad +(J_{s-1}^2 - J_{s+1}^2) \frac{z^2m^{-2}}{(s-\eta)^2} \frac{e^4-p^4x^4}{2p^2(1-x^2)} . \end{aligned} \tag{3.25}$$

Here the center-of-mass system is defined as:

$$p_1 = (e, p\sin\theta, 0, p\cos\theta) , \qquad p_2 = (e, -p\sin\theta, 0, -p\cos\theta) ,$$

$$k_1 = (e,0,0,-e)/(s-\eta) , \qquad k_2 = (e,0,0,e) ,$$

$$x = \cos\theta , \qquad s-\eta = \frac{s(e^2-p^2x^2)}{(e^2-p^2x^2)+\xi^2m^2} ,$$

$$z = \frac{2s\xi mp\sin\theta}{p^2\sin^2\theta + m^2(1+\xi^2)} . \tag{3.26}$$

Here, e, p and x are related to the laboratory quantities by

$$e^2 = \omega_1\omega_2(s-\eta) , \tag{3.27}$$

$$p = \sqrt{e^2-m^2} ,$$

$$\sin\theta = p_1\sin\theta_1/p , \tag{3.28}$$

$$\cos\theta = \sqrt{1-\sin^2\theta}\ \left(u-\frac{1}{2}\right) \Big/ \left|u-\frac{1}{2}\right| , \tag{3.29}$$

where $u = E_1/\omega_2$, with

$$u_{\substack{\max \\ \min}} = \frac{1}{2}\left[1 \pm \sqrt{1 - \frac{m^2(1+\xi^2)}{s\omega_1\omega_2}}\right] . \tag{3.30}$$

In Figs. 12 (a,b), we display the polarization of e^+ (or e^-) in the Compton limit ($\xi = 0.01, s = 1$) for low-energy ($\omega_1 = 15$ eV and $\omega_2 = 50$ GeV) and high-energy ($\omega_1 = 15$ eV and $\omega_2 = 500$ GeV) cases, respectively.

The functions A, B, and C are defined as

$$P(e^{\pm}) = \frac{P(k_1)A + P(k_2)B}{1 + P(k_1)P(k_2)C} , \tag{3.31}$$

where $P(e^{\pm})$, $P(k_1)$ and $P(k_2)$ are longitudinal polarizations of $e^{\pm}$, k_1 and k_2 respectively. From (a) and (b) we see that near the high-energy tip ($u \equiv E_1/\omega_2 \Rightarrow u_{\max}$), $P(e^{\pm})$ is determined mostly by $P(k_2)$. This is especially true at high energies.

Figure 12(c) gives the values of A, B, and C evaluated in the center-of-mass system. These curves are given purely for pedagogical purposes. The parameters used are the same as those for Fig. 12(a); namely, $\omega_1 = 15$ eV, $\omega_2 = 50$ GeV, and $\xi = 0.01$. The fact that A's (and B's) differ in two different frames are related to the Thomas precession [11]. It is easy to see that a particle having a spin parallel to its direction of motion is not a frame-independent concept if $m \neq 0$, because one can always go to the particle's rest frame and then boost it in a direction that is different from the spin direction. The $u = (u_{\max}, 0.5, u_{\min})$ correspond to $\cos\theta = (1, 0, -1)$. The A and B are mirror images of each other in the center-of-mass system, but not in the laboratory system. The values of A (or B) in both frames are similar at $u \to u_{\max}$ (i.e., $\theta \to 0$ in the C.M.), but they become opposite near

$u \to u_{\min}$ (i.e., $\theta \to \pi$ in the C.M.). This is easy to understand because if the spin of a particle is parallel to its direction of motion in the center-of-mass system, it will still be parallel near $u = u_{\max}$ in the laboratory system, but it will be antiparallel near $u = u_{\min}$ because the direction of motion is reversed by the Lorentz transformation. We also notice that C's are identical in two cases, because both the electron and positron spins are summed in D_{1s} and D_{2s} ($C = D_{2s}/D_{1s}$ with $s = 1$). The agreement in numerical values of C in two cases gives us a very welcome check on our calculation. We should remind the reader that the mass of the electron cannot be ignored in this problem because the center-of-mass energy is not high compared with m, even though both e^+ and e^- have energies of tens of GeV in the laboratory.

In Figs. 13(a,b) we plot D_{1s}, which gives the energy distributions for e^+ (or e^-). We notice that all the graphs are symmetric with respect to $u = 1/2$. This can be understood in the following way: the final state e^+e^- must be symmetric with respect to the exchange $e^+ \leftrightarrow e^-$ because it has a definite charge parity for a given s. Thus in the center-of-mass system where $e^+ \leftrightarrow e^-$ is equivalent to $\theta \to \pi - \theta$, the angular distribution must be symmetric with respect to $\theta = \pi/2$. According to Eqs. (3.4) and (3.28,3.29), $u = 1/2$ corresponds to $\theta = \pi/2$, and the reflection through $u = 1/2$ in the laboratory system is the same as reflection with respect to $\theta = \pi/2$ in the center-of-mass system. This explains the symmetry of these graphs with respect to $u = 1/2$. From these energy distributions we also notice that events are concentrated in the high energy and low energy ends. As the laser intensity (ξ) is increased, the range of u decreases for a given s [see Eq. (3.30)]; but events with large s participating become more prominent, and events with larger s have a larger range ($u_{\max} - u_{\min}$) of u.

The number of positron (or electrons) produced per incident high energy γ (labeled k_2) in the laser beam from l to $l+dl$ can be obtained from Eq. (3.18):

$$dW = dln_\gamma\sigma = \frac{\alpha dlm^2}{16\omega_2}\sum_{s=1}^{\infty}\int_{u_{\min}}^{u_{\max}} D_{1s}du\left(\frac{1}{197\times 10^{-13}\text{ cm MeV}}\right) , \tag{3.32}$$

where dl is the longitudinal path length of k_2 in laser in cm and n_γ is the number of photons per cm^3 of laser given by Eq. (A.3). We use the expression of D_{1s} given by Eq. (3.24) and $u_{\max}$ and $u_{\min}$ given by Eq. (3.30). Equation (3.32) can be simplified into

$$dW = 6.024\times 10^3\,\frac{dl\text{ (cm)}}{\omega_2\text{ (GeV)}}\sum_{s=1}^{\infty}\int_{u_{\min}}^{u_{\max}} D_{1s}\,du\ . \tag{3.33}$$

Inspection of numerical values of D_{1s} shown in Figs. 13(a,b) tells us that Eq. (3.33) can be valid only when $dl \ll 10^{-2}$ cm even for $\xi = 0.4$, otherwise dW is almost equal to unity or even exceeds it. Obviously, it is energetically impossible to create more than one high energy $e^\pm$ from one single high energy photon. Thus, attenuation of the k_2 beam as it goes through the laser beam must be taken into account.

Let L be the pulse length of the laser beam in cm ($\sim$ 0.05 cm, for example, used in Ref. [3]), then the total number of e^+ (or e^-) produced per incident k_2 with $u_{\min} < u < u_{\max}$ is

$$\begin{aligned} W &= \int_{u_{\min}}^{u_{\max}} du\int_0^L \exp\{-\sigma n_\gamma l\}\, n_\gamma\,\frac{d\sigma}{du}\,dl \\ &= (1-\exp\{-\sigma n_\gamma L\})\,\frac{1}{\sigma}\int_{u_{\min}}^{u_{\max}} du\,\frac{d\sigma}{du}\ . \end{aligned} \tag{3.34}$$

This shows that W can never exceed unity as expected and in our examples shown in Figs. 13 (a,b), W is nearly unity. Excessive laser intensity does not produce more $e^{\pm}$. We also notice that the attenuation does not affect the spectral shape of $e^{\pm}$. Summing the contribution from all s's, we see broadly speaking that there are two bumps in the spectrum, the high-energy bump and the low-energy bump. Equation (3.4) can be written

$$P_{1\perp}^2 = 4s\omega_1\omega_2\left[\frac{1}{4} - \left(u - \frac{1}{2}\right)^2\right] - m^2(1+\xi^2)$$

$$= 4s\omega_1\omega_2(u_{\max} - u)(u - u_{\min}) \tag{3.35}$$

where $P_{1\perp} = E_1\theta_1$ is the transverse momentum of $e^{\pm}$.

Equation (3.35) shows that the transverse momentum of $e^{\pm}$ is very small near $u = u_{\max}$ or $u = u_{\min}$, and the two bumps have identical $P_\perp$ distributions. For example, for $\omega_1 = 15\text{eV}$ and $\omega_2 = 50\text{GeV}$ we have

$$P_{1\perp}^2 = 35 \times 10^{12}(\text{eV})^2(u_{\max} - u)(u - u_{\min})\ ; \tag{3.36}$$

thus, near $u = u_{\max}$ or $u = u_{\min}$, we have $P_{1\perp} \leq m$.

In contrast to this, positrons are usually produced by impinging an electron beam on a tungsten target. The electron first produces bremsstrahlung in the target, and then the photon produces a pair. The direct electroproduction of a pair is usually negligible, being equivalent to about 0.02 radiation lengths of extra target thickness, according to the Weiszacher William's approximation [6]. The energy distribution of positrons by a monoenergetic incident electron on a target of t radiation lengths can be found in Tsai and Whitis [7]. The $P_\perp$ distribution is mostly due to multiple coulomb scattering

of the incident electron and the outgoing positron. The $P_\perp$ is given roughly by

$$< P_\perp >_{\rm ave} = 14.1 \text{ MeV}\sqrt{t} \ ,$$

where t is the sum of path lengths of the incident electron and the outgoing positron in radiation lengths in the target. For example, at SLAC the total radiator thickness is 6 rl. Part of this is traversed by the photon, so the effective t is $2 \sim 3$ rl. The average $P_\perp$ of e^+ from the pair production in a thick target is about 20 MeV, whereas from the laser it is less than 0.5 MeV. Thus, as a positron source, laser $+ \gamma \rightarrow e^+ + e^-$ is potentially much better than the existing method of using the thick target, provided that we have a free electron laser with sufficient intensity and a very high energy electron accelerator.

In Figs. 14–16 we show N_{1s}, N_{2s}, D_{1s}, and D_{2s} in the laboratory system for two sets of energies ($\omega_1 = 15$ eV, $\omega_2 = 50$ GeV and $\omega_1 = 15$ eV, $\omega_2 = 500$ GeV) and two laser intensities ($\xi = 0.4$ and $\xi = 1.0$). We make the following observations on these figures:

- Since D_{1s} is symmetric with respect to $u = 1/2$, there are an equal number of low- and high-energy $e^\pm$ clustered around $u_{\rm min}$ and $u_{\rm max}$.

- The polarization of k_2 and $e^\pm$ helicities are nearly the same near $u_{\rm max}$. The polarization of $e^\pm$ near $u_{\rm max}$ can be increased slightly if k_1 is made to have the same helicity as that of k_2, because N_{1s} and N_{2s} have the same sign near $u_{\rm max}$.

- Near $u = u_{\rm min}$, the quality of polarization is not so good. The polarization of $e^\pm$ near $u_{\rm min}$ is mostly determined by the polarization of k_1 (laser

beam) and their helicities are opposite. Again, if both k_1 and k_2 are polarized and have the same helicity, the polarization of $e^{\pm}$ near $u = u_{\min}$ will be slightly enhanced compared with having only k_1 polarized.

4. Polarized $e^{\pm}$ from Pair Production in an Atomic Target

Polarized $e^{\pm}$ from the photopair production was first investigated by Olsen and Maximon [8]. They included only the elastic atomic form factor. We include here the contribution from the inelastic atomic form factor in the manner of Wheeler and Lamb [9], using the Thomas-Fermi-Moliere model of atoms, which are suitable for atoms with $Z \geq 5$ (see Table B.2 of the author's Review of Modern Physics paper [6]).

Since the angular distribution of $e^{\pm}$ from pair production is caused mostly by the multiple Coulomb scattering, rather than by the production mechanism, the angle can be integrated out so that only the energy distribution is relevant. Both the energy distribution and the polarization of $e^{\pm}$ can be written in terms of four functions:

$$\varphi_1 = 20.863 - 2\ln(1+b^2) - 4b\arctan\left(\frac{1}{b}\right) - \frac{4}{3}\ln Z - 4f\ , \tag{4.1}$$

$$\varphi_2 = 20.196 - 2\ln(1+b^2) + 8b^2\left[1 - b\arctan\left(\frac{1}{b}\right) - 0.75\ln\left(1+\frac{1}{b^2}\right)\right] - \frac{4}{3}\ln Z - 4f\ , \tag{4.2}$$

$$\psi_1 = 28.340 - 2\ln(1+b'^2) - 4b'\arctan\left(\frac{1}{b'}\right) - \frac{2}{3}\ln Z\ , \tag{4.3}$$

$$\psi_2 = 27.673 - 2\ln(1+b'^2) + 8b'^2(1 - b'\arctan\left(\frac{1}{b'}\right) - 0.75(1+\frac{1}{b'^2}) - \frac{2}{3}\ln Z\ , \tag{4.4}$$

where

$$b = \frac{55.846 \text{ m}}{\left[ku(1-u)\ Z^{\frac{1}{3}}\right]}\ , \tag{4.5}$$

$$b' = \frac{362.01 \text{ m}}{\left[ku(1-u)\ Z^{\frac{2}{3}}\right]}\ , \tag{4.6}$$

are roughly $q_{\min} \times$ atomic radii for elastic and inelastic atomic form factors respectively [6]; f is the Coulomb correction to the one-photon exchange approximation worked out by Bethe and Maximon [10],

$$f(x) = 1.202\,x - 1.0369\,x^2 + \frac{1.008x^2}{1+x}\ , \tag{4.7}$$

where $x = (Z/137)^2$ and Z is the atomic number; k is the photon energy, and $u = E/k$ with E the energy of the $e^{\pm}$.

The differential cross section is then

$$\frac{d\sigma_p}{du} \ = \ \alpha\ r_0^2\ F\ , \tag{4.8}$$

where

$$F = Z^2\{(u^2+(1-u)^2)\varphi_1+\frac{2}{3}u(1-u)\varphi_2\}+Z\{(u^2+(1-u)^2)\psi_1+\frac{2}{3}u(1-u)\psi_2\}\ .$$

The polarization of $e^{\pm}$ is

$$P(e^{\pm}) = P(k)\ G\ , \tag{4.9}$$

where

$$G = \left[Z^2\{(2u-1)\varphi_1+\frac{2}{3}(1-u)\varphi_2\}+Z\{(2u-1)\psi_1+\frac{2}{3}(1-u)\psi_2\}\right]\Big/\ F\ ,$$

and P(k) is the polarization of the incident photon obtained by the backward-scattered laser beam defined by Eq. (2.17).

In Fig. 17(a) we have plotted $F/78400$ for $Z = 74$ (Tungsten). The number 78400 is a normalization factor in order to make the end points in the complete screening limit ($k = \infty$) equal to unity.

In Fig. 17(b) we plot the polarization of $e^{\pm}$, assuming the incident photon is completely right-hand polarized; i.e., $P(k) = 1$ in Eq. (4.9). The polarization is quite independent of energy—$k = 1$ GeV and $k = 20$MeV cases are plotted and they are hardly different. Near $u_{\max}$, the polarization is 100%; at $u = 0.9$, the polarization is 98%; at $u = 0.8$, it is 93%; and at $u = 0.7$, it is 84%. Suppose that we select the energy of $e^{\pm}$ so that only the $u > 0.7$ portion is accounted for, then the integrated polarization would be

$$\frac{\int_{0.7}^{1} P(e^{\pm})\, F\, du}{\int_{0.7}^{1} F\, du} . \tag{4.10}$$

This number would be more than 90% if we have almost 100% polarization for the incident photon beam.

5. Applications

1. Laser $(k_1) + e_-(p_1) \rightarrow k_2 + e_-(p_2)$ as a source of polarized photon beam. Compared with ordinary bremsstrahlung beam, the photon beam produced in this way has the following characteristics:

   (a) The spectrum here is peaked at both $u = u_{\max}$ and $u = 0$. This is to be compared with the bremsstrahlung spectrum, which is peaked only at $u = 0$ (the usual $1/k$ spectrum of bremsstrahlung [6]). See Figs. 3(a–c).

   (b) Due to the absence of Coulomb multiple scattering, the average transverse momentum of the photon here is $\leq m$, whereas

in the bremsstrahlung the average transverse momentum is approximately 14 MeV $\sqrt{t/2}$ where t is the radiator thickness in radiation lengths. This is important when one needs a beam that requires very small $P_\perp$.

(c) This process is relatively background free, whereas the ordinary bremsstrahlung is accompanied by many e^+e^- pairs and hadrons, especially when the target is thick.

(d) The $u_{\max}$ for bremsstrahlung is nearly 1, but for the laser electron scattering it can be much less than 1 if the center-of-mass momentum is much less than m. As the center-of-mass energy becomes much greater than m, $u_{\max}$ approaches 1. With the electron energy equal to 50 GeV, we need a Free Electron Laser in order to make $u_{\max}$ approach 1. See Eq. (2.34).

(e) Polarization. From the point of view of intensity and polarization, the most important region of the γ spectrum from the reaction laser + electron $\rightarrow \gamma$ + electron is within 20 to 30% of the tip of the spectrum for the lowest order ($s = 1$) mode. In this region, the contributions from $s \geq 2$ do not have good polarization if $4\omega_1 E_1 \leq m^2$. Thus, in this case, one should not let ξ be greater than 0.5 if good polarized γ beam is desired. One should increase the pulse length L in Eq. (2.31) rather than having a large ξ, in order to increase the yield of polarized photons. When $4\omega_1 E_1 \geq m^2(1+\xi^2)$, $u_{\max}$ approaches unity for all s; thus, good polarization for all s's can be obtained. In this case, a large value of ξ^2 can be used. See Eq. (2.34).

(f) When $4\omega_1 E_1 \ll m^2$, $u_{\max}$ is much less than 1. In this case, an electron can scatter laser photons many times, and we can thus produce many such scattered photons per incident electron. For example, when $E_1 = 10$ MeV and $\omega_1 = 1$ eV, we have $u_{\max} = 1.6 \times 10^{-4}$; thus, even after 600 consecutive scatterings by the laser photons, the electron would lose at most 9.6% of its energy. The scattered photons will have an energy of about 1.6 KeV on the high-energy side. This is definitely a better way to produce 1.6 KeV x-ray than the conventional way of producing x-rays.

2. Sources of Polarized $e^{\pm}$

(a) Method I: Laser$(k_1) + k_2 \rightarrow e^+(p_1) + e^-(p_2)$.

(b) Method II: $k_2 + Z \rightarrow e^+e^- + \cdots$.

(c) Existing Method

At the SLC at SLAC, a polarized e^- beam is produced by shining a polarized laser beam onto a GaAs Target [12]. The maximum polarization obtained up to now is 27% at the source and 22% at the interaction region where Z_0's are produced. The e^+ beam is not polarized. It is produced by impinging a 33 GeV electron beam onto a target of 6 rls [13]. Both e^+ and e^- beams are then accelerated and cooled in the cooling rings to reduce their temperature. They are then reinjected into the accelerator until they reach the final energy.

In Secs. 3 and 4 we discussed the characteristics of Method I and Method II, respectively. Method I requires very high energy back-scattered

photons (many tens of GeV) and a high-energy laser beam (> 10 eV) achievable only by the Free Electron Laser. In contrast, Method II requires only a backward-scattered photon beam with relatively low energy, because the threshold energy required is only a few MeV, 20 MeV photons will be more than adequate. See Fig. 17. The only disadvantage of Method II compared with Method I is the transverse momentum distribution due to multiple Coulomb scattering, but this problem is less serious here than in the existing method because the target thickness needed is less than one radiation length instead of six [13].

There are three reasons why we do not need, and do not want to have, a very thick radiator:

- The incoming particle is not an electron, but a photon.
- We are interested only in the first generation pair, the higher generation pairs do not possess desired polarizations.
- If the target is too thick, the $e^{\pm}$ produced will lose too much energy by bremsstrahlung.

According to Fig. 17(b) only the high-energy end ($u = 0.7$ to 1.0) has good polarization. Thus one must select this high-energy tip by a magnet before accelerating the beam.

Method I requires a Free Electron Laser, as well as a very high energy back-scattered polarized γ beam (many tens of GeV), to produce polarized $e^{\pm}$ beams. Its chief advantage is that the average transverse momentum is much less than m near $u_{\max}$ (at $u = u_{\max}$, we have $p_{\perp} = 0$). However,

this advantage may not be that significant, because the cooling rings can reduce the transverse momentum, as well as the spread in the longitudinal momentum of the beam.

The number of e^+ (or e^-) per incident electron in the energy interval dE using Method II can be written

$$dn_\pm = dE(1-\exp\{-n_\gamma\sigma_c L\})\,\frac{1}{\sigma_c}\int_E^{\omega_{2max}}\frac{d\sigma_c}{d\omega_2}\,d\omega_2\int_E^{\omega_2}\frac{d\sigma_p}{dE'}\,dE'$$
$$\times\int_0^T n\,\exp\{-\sigma_p n t\}\,I_e(E',E,T-t)\,dt\;; \qquad (5.1)$$

where n_γ is the number of laser photons per cm^3 introduced in Appendix A, and σ_c is the total Compton cross section:

$$\sigma_c = 2\pi r_0^2\,\frac{1}{w}\left\{\left(1-\frac{4}{w}-\frac{8}{w}\right)\ln(1+w)+\frac{1}{2}+\frac{8}{w}-\frac{1}{2(1+w)^2}\right\}\;, \qquad (5.2)$$

with $w = 4\omega_1 E_1/m^2$; ω_1 is the laser photon energy and E_1 is the incident electron energy in the reaction laser $(k_1) + p_1 \rightarrow k_2 + p_2$. L = laser pulse length in cm.

The first part of Eq. (5.1) up to the integration with respect to $d\omega_2$ is essentially Eq. (2.31), except that we have concluded that we should avoid the situation where $s \geq 2$ is significant, and thus the Compton cross section is used. The back-scattered photon with energy ω_2 then enters a target of total thickness T radiation lengths. The pair production takes place at the depth of t radiation length. The pair-production cross section $d\sigma_p/dE'$ is given by Eq. (4.8) where u is E'/ω_2; $n = \frac{N}{A}X_0$ is the number of target particles per unit radiation length; and $\exp(-\sigma_p n t)$ is the attenuation factor of the photon intensity at depth t. The total pair production cross section is given by

$$\sigma_p(k) = \sigma_p(\infty)[1-\zeta(k)]\;, \qquad (5.3)$$

where $\sigma_p(\infty) = (7/9)\ (A/X_0N)$ with A the atomic weight in grams/cm^2 and ζ the correction factor tabulated in Table IV.5 of Ref. [6]. The ζ can be obtained from integration of Eq. (4.8) and $I_e(E', E, T-t)$ is the straggling function of an electron whose energy is E' at production at depth t. The electron (or positron) then traverses the remaining target thickness $T-t$ to emerge from the target. Then $I_e(E', E, T-t)dE$ gives the energy distribution of an electron at T whose energy was E' at t. The straggling is caused by the bremsstrahlung emission (for simplicity, we ignore the straggling due to ionization and the Landau straggling [14]). The straggling function I_e can be written [15]

$$I_e\,(E', E, T-t) \;=\; \left[\ln\left(\frac{E'}{E}\right)\right]^{b(T-t)}\ \frac{d\sigma_b}{dk}\ \frac{N}{A}\ X_0(T-t)\ , \qquad (5.4)$$

where $k = E' - E$, X_0 is the unit radiation length of the target in g/cm^2, $d\sigma_b/dk$ is the bremsstrahlung cross section related to the pair-production cross section by the substitution rule [16]

$$\frac{d\sigma_b}{dk} = -(\frac{d\sigma_p}{dp})_{\substack{k\to -k\\ p\to -p}}\ \frac{k^2E}{p^3}\ , \qquad (5.5)$$

and $b \approx 4/3$.

Using Eq. (5.4), the t integration in Eq. (5.1) can be carried out analytically. We have

$$\int_0^T n\ \exp\{-\sigma_p n t\}\ I_e\,(E', E, T-t)\ dt \;=\; \frac{n^2}{\beta^2}\ \frac{d\sigma_b}{dk}[\epsilon^{\beta T}(\beta T - 1) + 1]e^{-\sigma_p n T}$$

$$\equiv\ H(E', E, T)\ , \qquad (5.6)$$

where $\beta = \sigma_p n + b\ln[\ln(E'/E)]$.

Similarly, the polarization of $e^{\pm}$ using Method II can be calculated by combining the polarization of the back-scattered photon in the Compton scattering with the polarization of $e^{\pm}$ in the pair production. Notice that:

(1) when the back-scattered photon passes through the target, its helicity is not changed, its intensity is changed because of the attenuation, and its energy distribution is slightly changed because the energy dependence of the σ_p in the absorption coefficient.

(2) the helicity of $e^{\pm}$ is not changed by bremsstrahlung or multiple Coulomb scattering as long as $e^{\pm}$ remains relativistic [17]. The polarization of $e^{\pm}$ at $t = T$, with energy E, is given by

$$P(e^{\pm}) = \frac{\int_E^{\omega_{2\max}} D_1 \, A d\omega_2 \int_E^{\omega_2} G(\omega_2, E') \, H(E', E, T) \, F(\omega_2, E') \, dE'}{\int_E^{\omega_{2\max}} D_1 \, d\omega_2 \int_E^{\omega_2} H(E', E, T) \, F(\omega_2, E') \, dE'}, \tag{5.7}$$

where D_1 is given by Eq. (2.24), A is given by N_1/D_1 with N_1 and D_1 given by Eq. (2.22) and (2.24) respectively, $G(\omega_2, E')$ is given by Eq. (4.9), $H(E', E, T)$ is given by Eq. (5.6), and $F(\omega_2, E')$ is given by Eq. (4.8).

6. Concluding remarks

When dealing with a problem in which many particles are polarized, it is easier to deal with calculation of matrix elements directly, instead of matrix elements squared, using density matrices and projection operators. This is true even when dealing with the simplest problem, such as the lowest order Compton scattering. When the matrix element itself is very complicated, the square of it becomes hopelessly complicated. It is often more convenient, or even unavoidable, to calculate the amplitude directly. This paper demonstrates how to deal with the transition amplitude directly using MAPLE. For the lowest order Compton scattering, our Eqs. (2.22) through (2.25) reproduce the results given by Lipps and Tolhoek [19], who also gives earlier references on the subject.

Acknowledgments

The author would like to thank R. Palmer and James Spencer for getting him interested in this subject; Marvin Weinstein for teaching him how to use MAPLE; and Stan Ecklund, Allen Odian, and Francesco Villa for discussions on possible applications of this investigation. The author is most grateful to the anonymous referee who not only pointed out a mistake in the original manuscript, but also derived Eq. (2.44).

References

1. D. M. Volkov, Z. F. Phys. **94**, 250 (1935), quoted by Berestetskii, Lifshitz, and Pitaevskii in § 40 and § 101 of *Quantum Electrodynamics* (Pergamon Press, New York, 1980).

2. N. B. Narozhmyi, A. I. Nikishov, and V. I. Ritus, Soviet Physics JETP **20**, 622 (1965).

3. K. T. McDonald et al., "Study of QED at critical field strength," a letter of intent to SLAC, August 1991.

4. "Maple V" by Bruce Char et al., (Spring-Verlag, New York, 1991).

5. Equation (101.15) of Ref. [1] has a wrong dimension defined there: W cannot be the total probability of emission from unit volume in unit time. It is actually the total number of scattered photons per incident electron per unit length of laser pulse length, assuming the laser pulse length is infinitesimal so that the attenuation treated here can be ignored.

6. Y. S. Tsai, Rev. Mod. Physics **46**, 815 (1974), Eqs. (4.21) and (4.23).

7. Y. S. Tsai and Van Whitis, Phys. Rev. **149**, 1248 (1966).

8. H. Olson and L. L. Maximon, Phys. Rev. **114**, 887 (1959). See also A. Claesson, Ark. Fysik **12**, 569 (1957).

9. J. A. Wheeler and W. E. Lamb, Jr., Phys. Rev. **55**, 858 (1939) and **101E**, 1834 (1956).

10. H. A. Bethe and L. C. Maximon, Phys. Rev. **93**, 768 (1954).

11. See, for example, § 22 of C. Moller, "The Theory of Relativity," (Oxford, 1955).

12. J. E. Clendenin, "The SLAC Polarixed Electron Source," presented at the 1990 Workshop on Polarized Electron Sources and Electron Spin Polarimeters, Bonn, Germany; SLAC–PUB– 5368 (1990).

13. R. Pitthan et al., "SLC Positron Source—Simulation and Performance," presented at the 1991 IEEE Accel. Conf., San Francisco; SLAC–PUB–5547 (1991).

14. Since we are dealing with $e^{\pm}$ beam whose energy is $10 \sim 20$ MeV, the Landau straggling and the energy loss due to ionization become non-negligible. The best account of combined effects of bremsstrahlung, ionization, and Landau straggling can be found in Appendix B of Y. S. Tsai, "Radiative Corrections to Electron Scattering," SLAC–PUB–848 (1971).

15. Y. S. Tsai, Rev. Mod. Physics **46**, 815 (1974), Eq. (4.5).

16. *ibid.*, Eq. (3.79).

17. C. K. Iddings, G. L. Shaw and Y. S. Tsai, Phys. Rev. **135B**, 1388 (1964).

18. J. D. Bjorken and S. D. Drell *Relativistic Quantum Fields,* (McGraw-Hill, New York, 1965).

19. F. W. Lipps and H. A. Tolhoek, Physica **20**, 395 (1954).

Appendix A. Intensity of Laser Beam and the Parameter ξ

The dimensionless parameter ξ is related to the intensity of the laser beam. The energy density of the electromagnetic field is

$$W = \frac{E^2 + H^2}{2} = E^2 = a^2\omega_1^2 ,$$

where the electric field $\vec{E}$ is related to $\vec{A}$ in the radiation gauge ($A_0 = 0$) by $\left|\vec{E}\right| = \left|\partial\vec{A}/\partial t\right| = a\omega_1$.

The number of photons per cm^3 is thus

$$n_\gamma = \frac{W}{\omega_1} = a^2\omega_1 , \tag{A.1}$$

and

$$\xi^2 \equiv \frac{\alpha a^2 4\pi}{m^2} = n_\gamma \left(\frac{4\pi\alpha}{m^2\omega_1}\right) . \tag{A.2}$$

Since ξ is dimensionless and m and ω_1 are usually given in electron volts we have to convert "per cm^3" in the definition of n_γ into electron volts (eV^3) by the relation

$$1 = \hbar c = 197.3 \times 10^{-7} \text{ eVcm} .$$

Thus

$$\xi^2 = n_\gamma \frac{4\pi\alpha(197.3 \times 10^{-7} \text{ eV})^3}{m^2\omega_1} . \tag{A.3}$$

The laser intensity is usually given in units of W/cm^2. It is related to the photon density by

$$I \text{ (W/cm}^2\text{)} = n_\gamma \, 4.8 \times 10^{-9}\omega_1 \text{ (eV) W/cm}^2 .$$

We finally obtain

$$\xi^2 = \frac{I(\text{W/cm}^2)}{[\omega_1 \text{ (eV)}]^2} \, 5.64 \times 10^{-19} . \tag{A.4}$$

Appendix B. Spinors for Helicity States and the Use of Maple

MAPLE is a very generic computer program which can handle both analytical and numerical manipulations, but it is not specifically written for high-energy physics. Therefore, we have to write down explicit representations for γ matrices as well as for the spinors, and let the computer do the matrix multiplications. In this paper we adopt the explicit representation of Gamma matrices and the metric used by Bjorken and Drell in Ref. [18]. The explicit representations for the helicity states for spin-1/2 particles and antiparticles with mass m with four momentum $p_\mu = (e,\, p\sin\theta\cos\varphi\,, p\sin\theta\sin\varphi,\, p\cos\theta)$ are:

$$u\left(p,\theta,\varphi,\frac{1}{2}\right) = c_1 \begin{bmatrix} \cos(\theta/2) \\ e^{i\varphi}\sin(\theta/2) \\ c_2\,\cos(\theta/2) \\ c_2\,e^{i\varphi}\sin(\theta/2) \end{bmatrix} \equiv u_+\,, \tag{B.1}$$

$$u\left(p,\theta,\varphi,-\frac{1}{2}\right) = c_1 \begin{bmatrix} -e^{-i\varphi}\sin(\theta/2) \\ \cos(\theta/2) \\ c_2\,e^{-i\varphi}\sin(\theta/2) \\ -c_2\cos(\theta/2) \end{bmatrix} \equiv u_-\,, \tag{B.2}$$

$$v\left(p,\theta,\varphi,\frac{1}{2}\right) = c_1 \begin{bmatrix} c_2\,e^{-i\varphi}\sin(\theta/2) \\ -c_2\cos(\theta/2) \\ -e^{-i\varphi}\sin(\theta/2) \\ \cos(\theta/2) \end{bmatrix} \equiv v_+\,, \tag{B.3}$$

$$v\left(p,\theta,\varphi,-\frac{1}{2}\right) = c_1 \begin{bmatrix} c_2\cos(\theta/2) \\ c_2\,e^{i\varphi}\sin(\theta/2) \\ \cos(\theta/2) \\ e^{i\varphi}\sin(\theta/2) \end{bmatrix} \equiv v_-\,, \tag{B.4}$$

where $c_1 = (e+m)^{1/2}$, $c_2 = p/(e+m)$, and $(\pm 1/2)$ denotes the positive and negative helicities.

The spinors with a bar are defined as usual, $\bar{u} = u^+\gamma_0$ and $\bar{v} = v^+\gamma_0$, where $^+$ denotes the hermitian conjugate. Each of the four spinors given

above is defined as a procedure in MAPLE, so that we can apply it to represent a fermion with any p, m, θ, φ, and helicity. It should be noted that the phase factor in each of the eight spinors defined above is not relevant to our problem, because two different helicity amplitudes do not interfere with one another, and only the square of each helicity amplitude contributes to the polarization and the differential cross sections.

The spinor representations shown above are obtained in the following way:

From Dirac equations $(\not{p} - m)u = 0$, we obtain

$$u_{\pm} = c_1 \begin{bmatrix} \chi_{\pm} \\ \\ \frac{\vec{p}\cdot\vec{\sigma}}{e+m}\,\chi_{\pm} \end{bmatrix} , \tag{B.5}$$

where χ_+ is a 2×1 spinor representing an electron with spin parallel to $\vec{p}$ (or antiparallel when $-$) in its rest frame, and c_1 is the normalization factor so that $\bar{u}u = 2m$ and $\bar{v}v = -2m$. An explicit expression for $\chi_{\pm}$ can be obtained by solving $\vec{p}\cdot\vec{\sigma}\chi_{\pm} = \pm p\chi_{\pm}$; we have

$$\chi_+ = \begin{bmatrix} \cos(\theta/2) \\ \\ \sin(\theta/2)\, e^{i\varphi} \end{bmatrix} \quad \text{and} \quad \chi_- = \begin{bmatrix} -\sin(\theta/2)\, e^{-i\varphi} \\ \\ \cos(\theta/2) \end{bmatrix} . \tag{B.6}$$

Since the overall phase is not relevant, we have chosen the form which is the simplest. v_+ and v_- can be obtained by the change conjugation of u_+ and u_-:

$$v_+ = i\gamma_2 u_+^* \quad \text{and} \quad v_- = -i\gamma_2 u_-^* .$$

Again the phases of v_+ and v_- are arbitrarily chosen.

The final check on the validity of our expressions for $u_{\pm}$ and $v_{\pm}$ can be performed using the relations

$$\gamma_5 \not{s} u_{\pm} = \pm u_{\pm} , \tag{B.7}$$

and

$$\gamma_5 \not{s} v_\pm = \pm v_\pm \ , \tag{B.8}$$

where s is a four vector having the components:

$$s_\mu = \left[p/m \ , \quad \frac{e}{m} \sin\theta\cos\varphi \ , \quad \frac{e}{m} \sin\theta\sin\varphi \ , \quad \frac{e}{m} \cos\theta \right] \ .$$

This check shows that indeed $u_\pm$ (and $v_\pm$) represent states with helicity $\pm$.

Since MAPLE handles both analytic and numerical manipulations, we must decide how much we should let the computer do the analytical work and at what stage we should do numerical computations. In general, if one can obtain a simple analytical expression to describe nature, then one should obtain this expression, but if the expression is too lengthy and complicated, then we should be satisfied with numerical results.

In this paper we obtained analytical expressions for differential cross sections for both reactions given in the title, as well as the photon polarization in the first reaction, but we have to be satisfied with only numerical results for the polarization of $e_\pm$ in the second reaction. The reason is that the differential cross section and the photon polarization have invariant meaning, and thus can be calculated in any convenient coordinate system, but the helicity of a particle with nonzero mass does not have invariant meaning and thus can be calculated only in the frame where it is going to be observed (we call this the laboratory system in this paper which is different from customary usage where one of the incident particles is at rest).

Nevertheless, for pedagogical reasons we have also calculated the polarization of $e^\pm$ in the second reaction in the center-of-mass system [see Fig.10(c)], which is to be compared with that in the laboratory system [Fig.

10(a)]. This serves as a textbook illustration of the fact that two successive Lorentz boosts, not in the same direction, result in a Lorentz boost times a rotation. This phenomenon is usually treated in textbooks [11] under Thomas Precession. The illustration given here is easier to grasp than the Thomas Precession.

Appendix C. Compton Scattering in the $p_1 = (m, 0, 0, 0)$ System

Let us denote the incident photon energy and the photon scattering angle in the rest frame of the initial electron by k_1^* and θ^* respectively. We further define K=k_1^*/m and $X = cos\theta^*$. We have then

$$y^2 = 1 + 2K, \tag{c.1}$$

$$x = ((K+1)X - K)/(1 + K(1-X)). \tag{c.2}$$

Substituting these expressions into Eqs.(2.22) through (2.25) we obtain

$$N_1 = 2\xi^2 X(K^2X^2 - 2(K^2+K)X + K^2 + 2K + 2)/D, \tag{c.3}$$

$$N_2 = 2\xi^2(1-X)K(X^2 - KX + K + 1)/D, \tag{c.4}$$

$$D_1 = 2\xi^2(-KX^3 + (K^2+K+1)X^2 - (2K^2+K)X + K^2 + K + 1)/D, \tag{c.5}$$

$$D_2 = 2\xi^2 XK(KX^2 - (2K+2)X + K + 2)/D, \tag{c.6}$$

where D=-KX+K+1.

For the laser+high energy electron back scattering these expressions can also be written in the more convenient variables $u = \omega_2/E_1$ and $w = 4\omega_1 E_1/m^2 = u_{max}$ using the relations

$$K = w/2, \tag{c.7}$$

$$X = 1 - 2u/(w - wu). \tag{c.8}$$

We have

$$N_1 = 2\xi^2(2 - 2u + u^2)(1 - \frac{2u}{(1-u)w})/(1-u) \tag{c.9}$$

$$N_2 = 2\xi^2(-\frac{(2-u)u}{1-u} + \frac{4u^2}{(1-u)w} + \frac{4u^3}{(1-u)^2w^2}), \qquad (c.10)$$

$$D_1 = 2\xi^2(\frac{2-2u+u^2}{1-u} - \frac{4u}{(1-u)w} + \frac{4u^2}{(1-u)^2w^2}), \qquad (c.11)$$

$$D_2 = 2\xi^2\frac{u(2-u)}{1-u}(1 - \frac{2u}{(1-u)w}). \qquad (c.12)$$

In the Thomson limit we have $K \ll 1$, $w \ll 1$, $u \ll 1$, and $X \to (1 - \frac{2u}{w})$, thus

$$N_1 \to 4\xi^2 X = 4\xi^2(1 - \frac{2u}{w}), \qquad (c.13)$$

$$N_2 \to 0,$$

$$D_1 \to 2\xi^2(1 + X^2) = 4\xi^2(1 - \frac{2u}{w} + \frac{2u^2}{w^2}), \qquad (c.14)$$

$$D_2 \to 0.$$

Eqs. (c.3), (c.6), (c.9) and (c.12) show explicitly that the origin for the zeros for N_1 and D_2 is due to θ^* being equal to $\pi/2$. Our Eqs. (c.3) through (c.6) agree with the results given by Lipps and Tolhoek[19].

Figure Captions

1. Feynman diagrams for the reaction laser $(k_1\lambda_1)$+ electron $(p_1\lambda_4) \to$ photon $(k_2\lambda_2)$+ electron $(p_2\lambda_3)$.

2. The center-of-mass system for the reaction laser + electron $\to$ photon + electron, $(s-\eta)\vec{k}_1 + \vec{p}_1 = \vec{k}_2 + \vec{p}_2 = 0$.

3. Energy distribution and polarization of the scattered photon in the Compton scattering where $u = \omega_2/E_1$, D_1 is the energy distribution of the scattered photon given by Eq. (2.24), and A, B, and C are the parameters for polarization defined by Eq. (2.38) for (a) $\omega_1 = 3.5$ eV,

$E_1 = 1$ GeV; (b) $\omega_1 = 1.17$ eV, $E_1 = 50$ GeV; and (c) $\omega_1 = 3.5$ eV, $E_1 = 500$ GeV.

4. This graph illustrates that the polarization of scattered photons is slightly enhanced if the incident electron is also polarized, in addition to the incident laser whose polarization is the primary factor, with $\omega_1 = 1.17$ eV, $E_1 = 50$ GeV, and $\xi = 0.01$.

5. Reaction $sk_1 + p_1 \rightarrow k_2 + p_2$ for a strong laser beam ($\xi = 1$) with $\omega_1 = 3.5$ eV and $E_1 = 1$ GeV, for (a) energy distribution, D_{1s} given by Eq. (2.20) , and (b) polarization, N_{1s} given by Eq. (2.18).

6. The N_{1s}, N_{2s}, D_{1s}, and D_{2s} for laser-electron scattering as given by Eqs. (2.18)–(2.21), with $\omega_1 = 1.17$ eV, $E_1 = 50$ GeV, and $\xi = 0.4$ for (a) $s = 1$, (b) $s = 2$, and (c) $s = 3$.

7. The N_{1s}, N_{2s}, D_{1s}, and D_{2s} for laser-electron scattering as given by Eqs. (2.18)–(2.21), with $\omega_1 = 1.17$ eV, $E_1 = 50$ GeV, and $\xi = 1.0$ for (a) $s = 1$, (b) $s = 2$, and (c) $s = 3$.

8. The N_{1s}, N_{2s}, D_{1s}, and D_{2s} for laser-electron scattering as given by Eqs. (2.18)—(2.21) with $\omega_1 = 3.5$ eV, $E_1 = 500$ GeV, and $\xi = 0.4$ for (a) $s = 1$, (b) $s = 2$, and (c) $s = 3$.

9. The N_{1s}, N_{2s}, D_{1s} and D_{2s} for laser-electron scattering as given by Eqs. (2.18)–(2.21) with ω_1=3.5 eV, $E_1 = 500$ GeV, $\xi = 1.0$ for (a) $s = 1$, (b) $s = 2$, and (c) $s = 3$.

10. Feynman diagrams for the reaction laser $(k_1\lambda_1)$ + photon$(k_2\lambda_2) \rightarrow$ electron$(p_1\lambda_4)$ + positron$(p_2\lambda_3)$.

11. Kinemetics for laser $(sk_1) + k_2 \rightarrow e^+(p_1) + e^-(p_2)$. All momenta and angles refer to the laboratory system.

12. Polarization of $e^\pm$ in Laser$+\gamma \rightarrow e^+e^-$ where A, B and C are defined by Eq. (3.31) and $u = E_1/\omega_2$ in the laboratory system for (a) $\omega_1 = 15$ eV, $\omega_2 = 50$ GeV, $s = 1$, and$\xi = 0.01$; for (b) $\omega_1 = 15$ eV, $\omega_2 = 500$ GeV, $s = 1$, and $\xi = 0.01$; and (c) for polarization of $e^\pm$ in the center-of-mass system for $\omega_1 = 15$ eV, $\omega_2 = 50$ GeV, $s = 1$, and $\xi = 0.01$.

13. Energy distribution of $e^\pm$ in the laboratory system for laser$+\gamma \rightarrow e^+ + e^-$ with $u = E_1/\omega_2$. Curves plotted are for D_{1s} given by Eq. (3.24) for (a) $\omega_1 = 15$ eV, $\omega_2 = 50$ GeV, $\xi = 0.4$, and for (b) $\omega_1 = 15$ eV, $\omega_2 = 50$ GeV, $\xi = 1.0$.

14. The N_{1s}, N_{2s}, D_{1s}, and D_{2s} for Laser$+\gamma \rightarrow e^+e^-$ as given by Eqs. (3.17)–(3.20) with $\omega_1 = 15$ eV, $W_2 = 50$ GeV, $\xi = 0.4$ for (a) $s = 1$, (b) $s = 2$, and (c) $s = 3$.

15. The N_{1s}, N_{2s}, D_{1s}, and D_{2s} for Laser$+\gamma \rightarrow e^+e^-$ as given by Eqs. (3.17)–(3.20) with $\omega_1 = 15$ eV, $\omega_2 = 50$ GeV, and $\xi = 1.0$ for (a) $s = 1$, (b) $s = 2$, (c)'$s = 3$.

16. The N_{1s}, N_{2s}, D_{1s}, and D_{2s} for Laser$+\gamma \rightarrow e^+e^-$ as given by Eqs. (3.17)–(3.20) with $\omega_1 = 15$ eV, $\omega_2 = 500$ GeV, $\xi = 1.0$ for (a) $s = 1$, (b) $s = 2$, (c) $s = 3$.

17. (a) The energy distribution of $e^\pm$ from $k + Z \rightarrow e^+e^- \cdots$, where Z is a Tungsten target and $u = E_\pm/k$, and (b) the polarization of $e^\pm$ from $k + Z \rightarrow e^+e^- \cdots$. Curves plotted represent $P(e^\pm)/P(k)$ for $k = 20$ MeV and $k = 1.0$ GeV respectively.

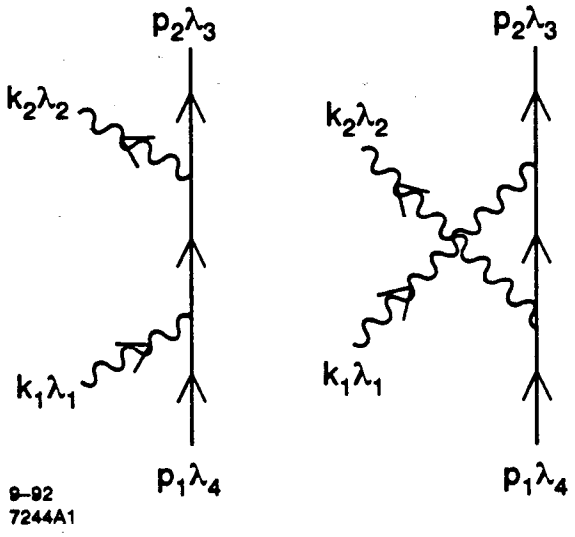
$p_2\lambda_3$
$k_2\lambda_2$
$k_1\lambda_1$
$p_1\lambda_4$
$p_2\lambda_3$
$k_2\lambda_2$
$k_1\lambda_1$
$p_1\lambda_4$
9-92
7244A1

Fig.1

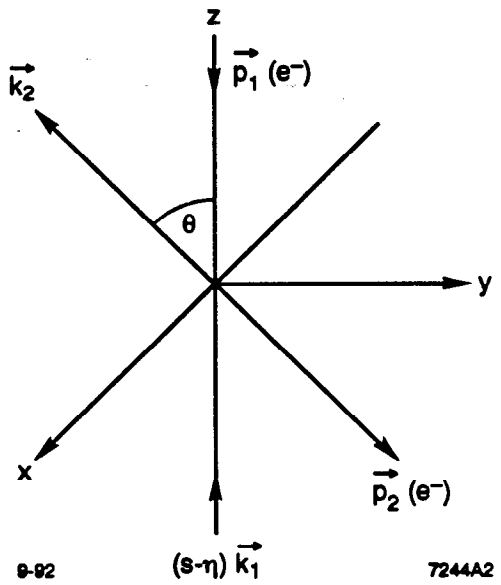

Fig.2

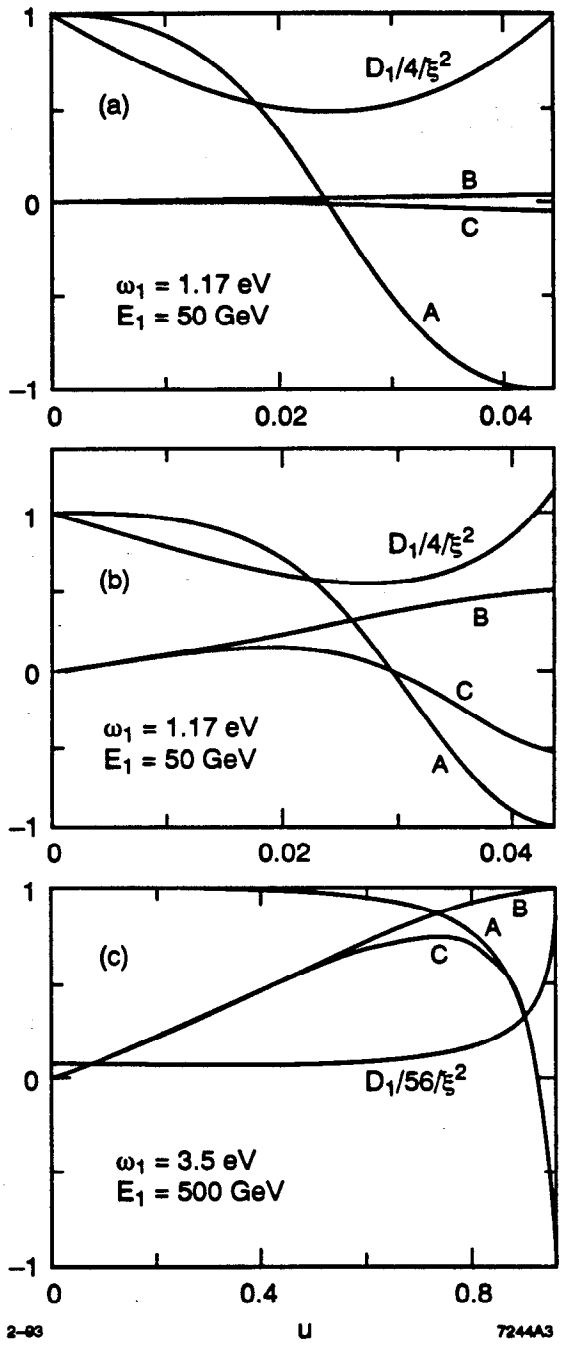
1
0
−1
0
0.02
0.04
(a)
$D_1/4/\xi^2$
B
C
A
ω_1 = 1.17 eV
E_1 = 50 GeV
(b)
$D_1/4/\xi^2$
B
C
A
ω_1 = 1.17 eV
E_1 = 50 GeV
(c)
B
A
C
$D_1/56/\xi^2$
ω_1 = 3.5 eV
E_1 = 500 GeV
0.4
0.8
2-93
U
7244A3

Fig. 3

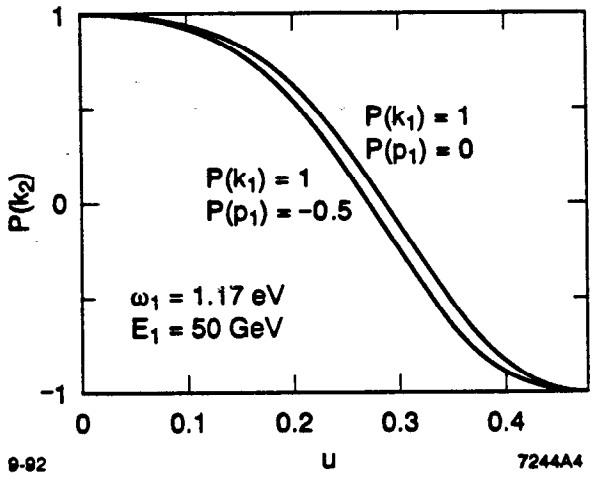
1
0
−1
P(k2)
0
0.1
0.2
0.3
0.4
u
P(k1) = 1
P(p1) = 0
P(k1) = 1
P(p1) = −0.5
ω1 = 1.17 eV
E1 = 50 GeV
9-92
7244A4

Fig.4

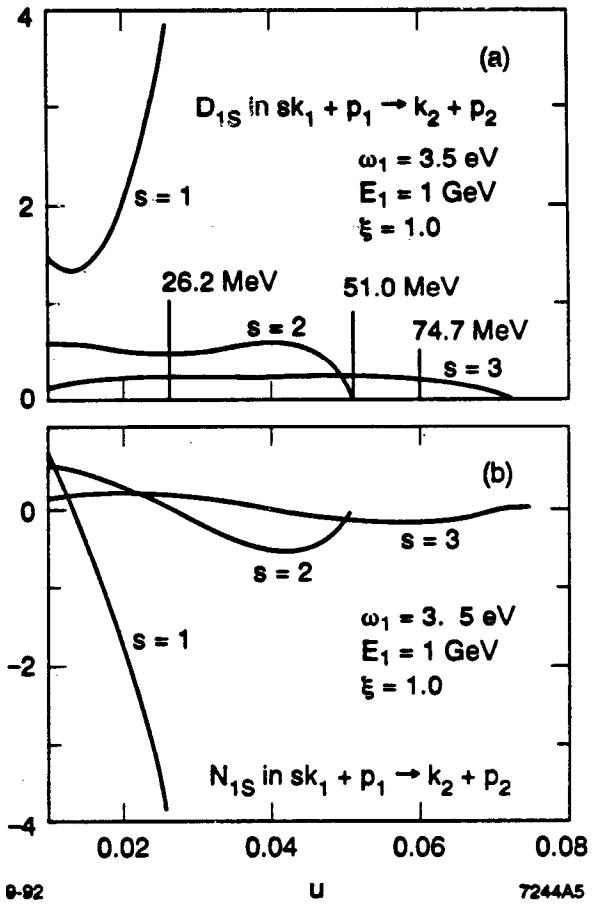
(a)
D_{1S} in $sk_1 + p_1 \rightarrow k_2 + p_2$
ω_1 = 3.5 eV
E_1 = 1 GeV
ξ = 1.0
s = 1
26.2 MeV
51.0 MeV
s = 2
74.7 MeV
s = 3
(b)
s = 3
s = 2
s = 1
ω_1 = 3. 5 eV
E_1 = 1 GeV
ξ = 1.0
N_{1S} in $sk_1 + p_1 \rightarrow k_2 + p_2$
4
2
0
-2
-4
0.02
0.04
0.06
0.08
u
9-92
7244A5

Fig.5

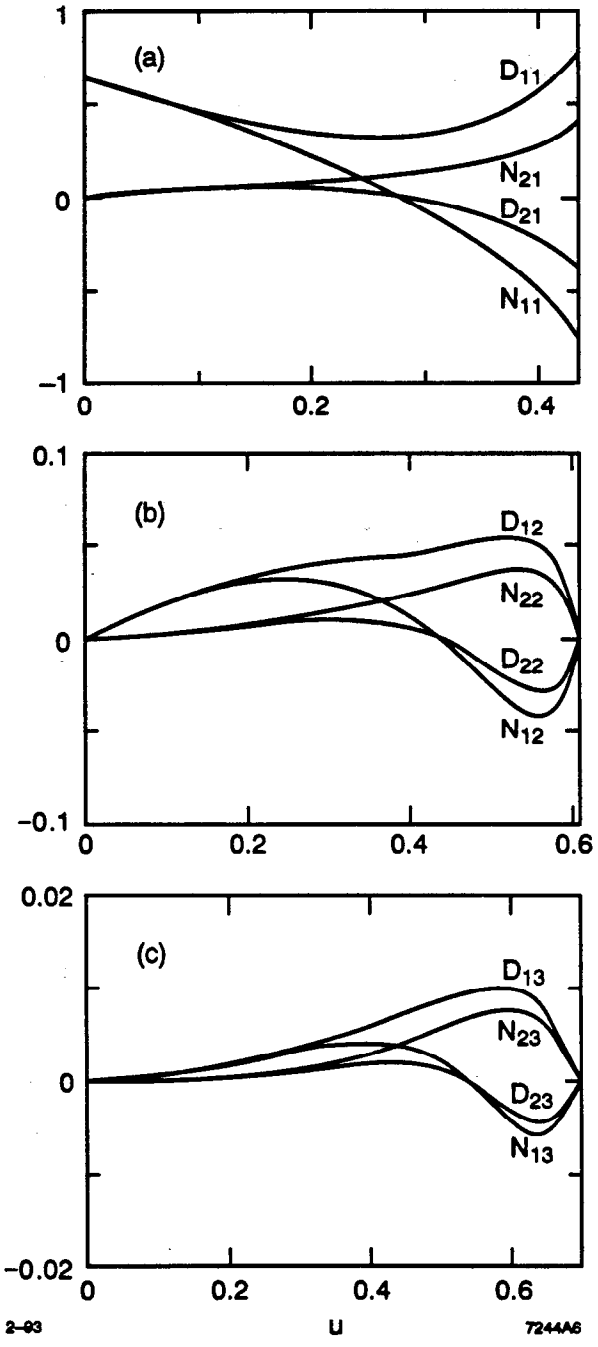
(a)
D_{11}
N_{21}
D_{21}
N_{11}
1
0
−1
0
0.2
0.4
(b)
D_{12}
N_{22}
D_{22}
N_{12}
0.1
0
−0.1
0
0.2
0.4
0.6
(c)
D_{13}
N_{23}
D_{23}
N_{13}
0.02
0
−0.02
0
0.2
0.4
0.6
2-93
u
7244A6

Fig. 6

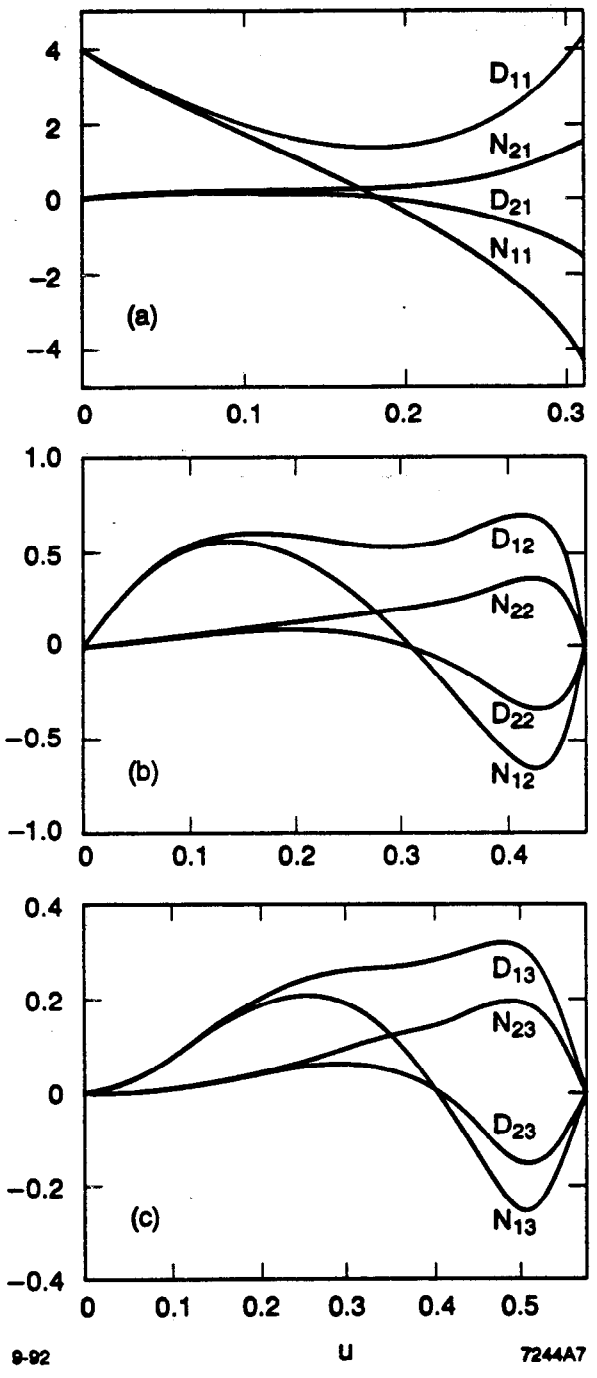
4
2
0
−2
−4
D11
N21
D21
N11
(a)
0
0.1
0.2
0.3
1.0
0.5
0
−0.5
−1.0
D12
N22
D22
N12
(b)
0
0.1
0.2
0.3
0.4
0.4
0.2
0
−0.2
−0.4
D13
N23
D23
N13
(c)
0
0.1
0.2
0.3
0.4
0.5
u
9-92
7244A7

Fig.7

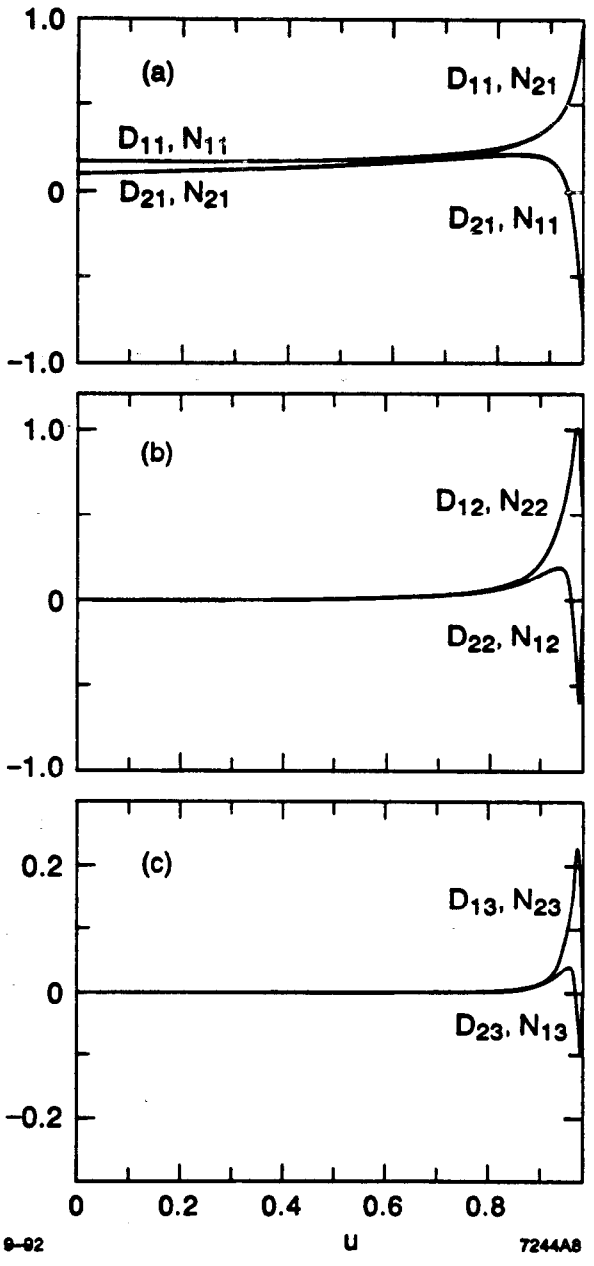
1.0
(a)
D11, N21
D11, N11
0
D21, N21
D21, N11
-1.0
1.0
(b)
D12, N22
0
D22, N12
-1.0
0.2
(c)
D13, N23
0
D23, N13
-0.2
0
0.2
0.4
0.6
0.8
u
9-92
7244A8

Fig.8

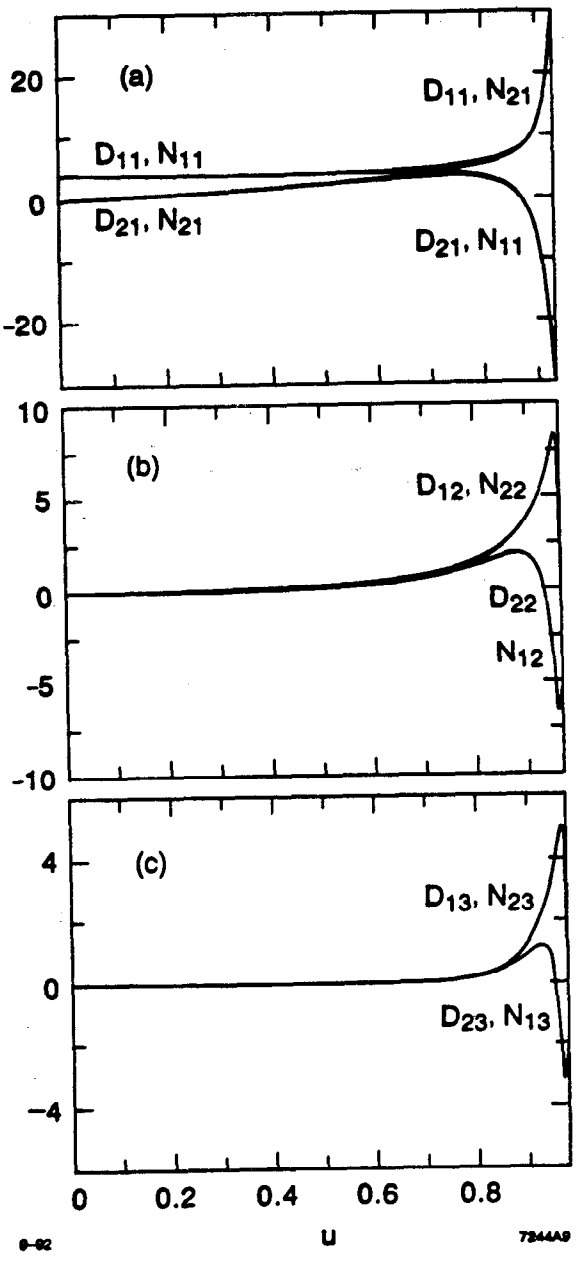
20
(a)
D_{11}, N_{21}
D_{11}, N_{11}
0
D_{21}, N_{21}
D_{21}, N_{11}
-20
10
(b)
D_{12}, N_{22}
5
0
D_{22}
N_{12}
-5
-10
4
(c)
D_{13}, N_{23}
0
D_{23}, N_{13}
-4
0
0.2
0.4
0.6
0.8
u
8-92
7844A9

Fig.9

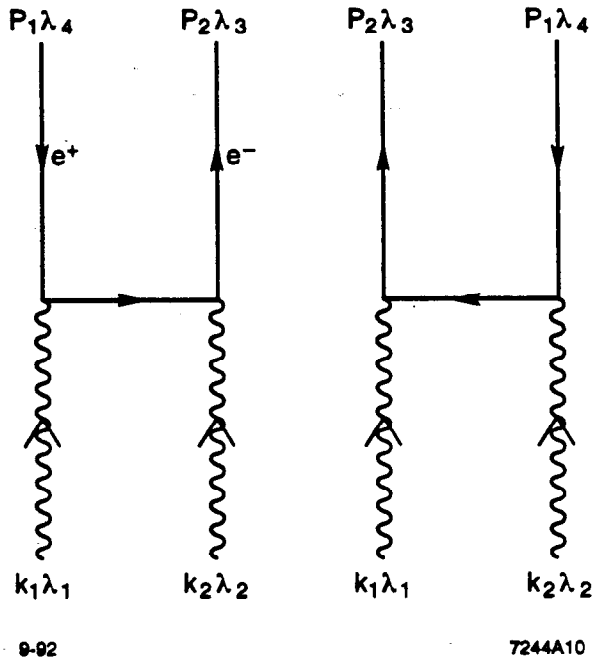

Fig.10

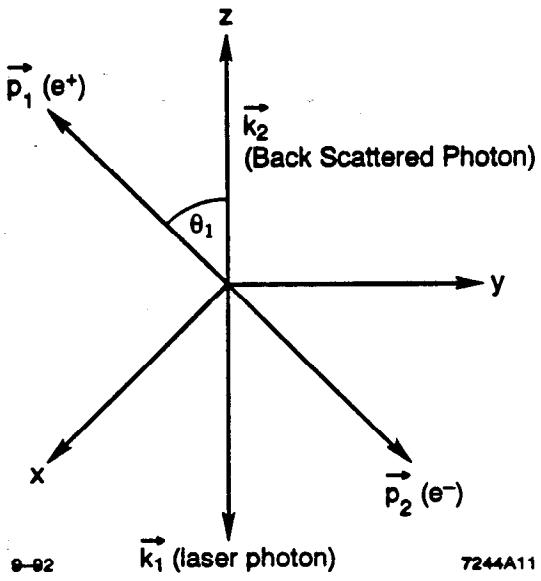
z
$\vec{p}_1$ (e^+)
$\vec{k}_2$
(Back Scattered Photon)
θ_1
y
x
$\vec{p}_2$ (e^-)
$\vec{k}_1$ (laser photon)
9-92
7244A11

Fig.11

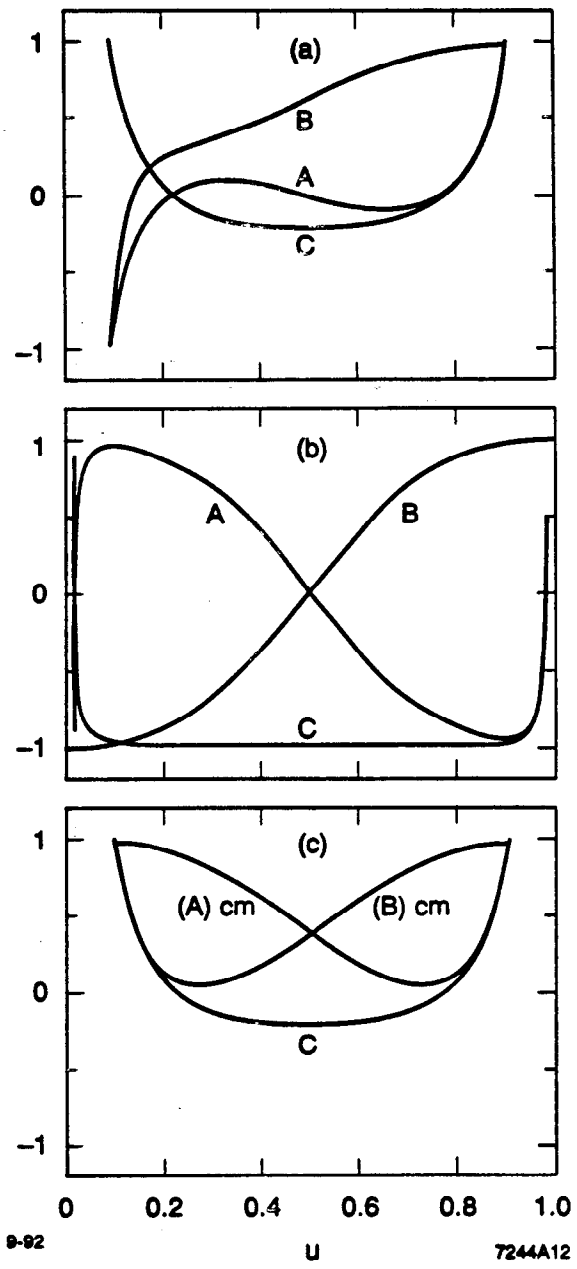

Fig.12

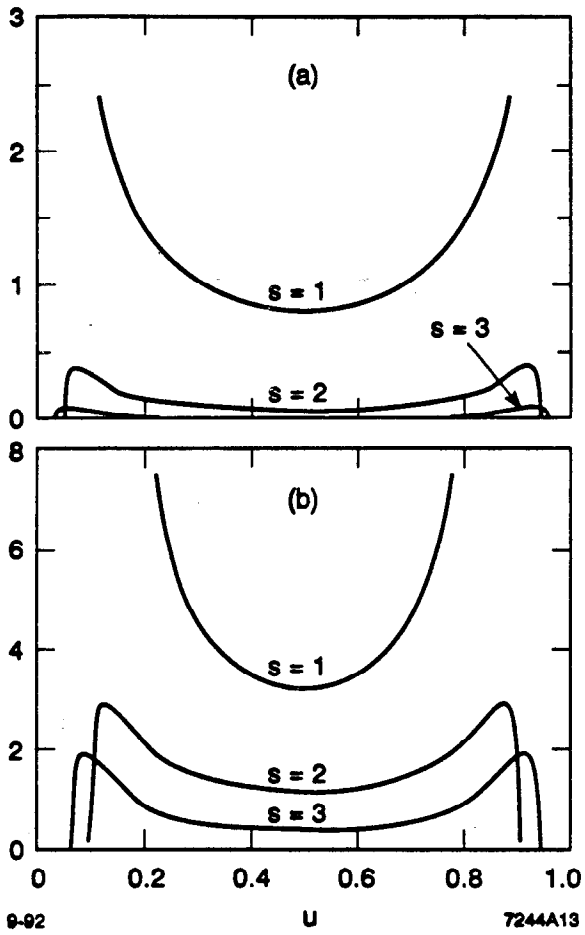

Fig.13

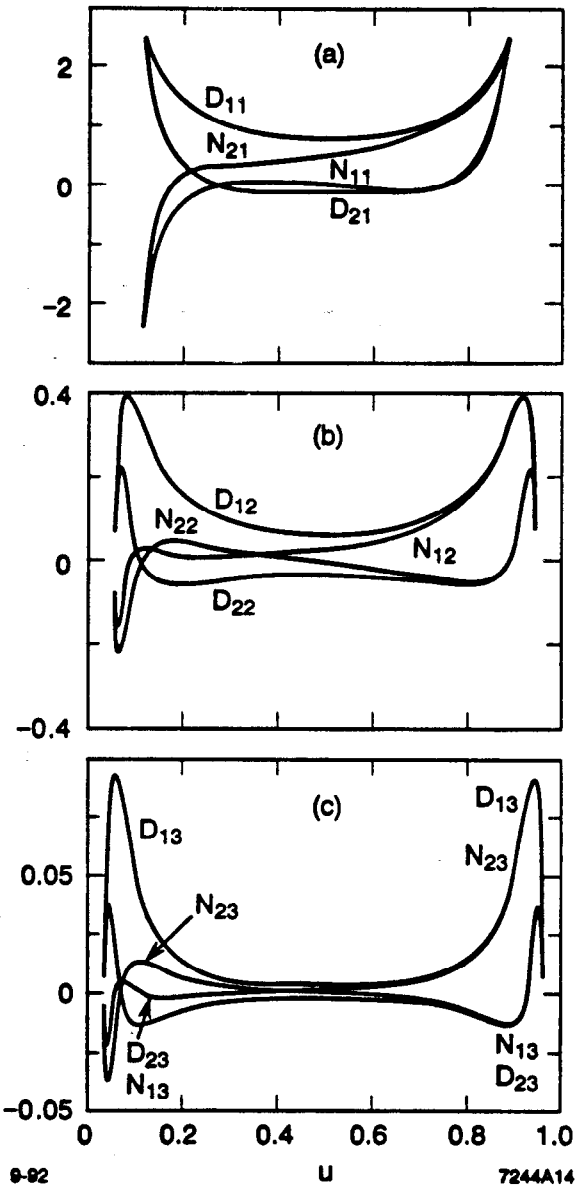
(a)
2
0
-2
D_{11}
N_{21}
N_{11}
D_{21}
(b)
0.4
0
-0.4
D_{12}
N_{22}
N_{12}
D_{22}
(c)
0.05
0
-0.05
D_{13}
N_{23}
D_{23}
N_{13}
0
0.2
0.4
0.6
0.8
1.0
u
8-92
7244A14

Fig.14

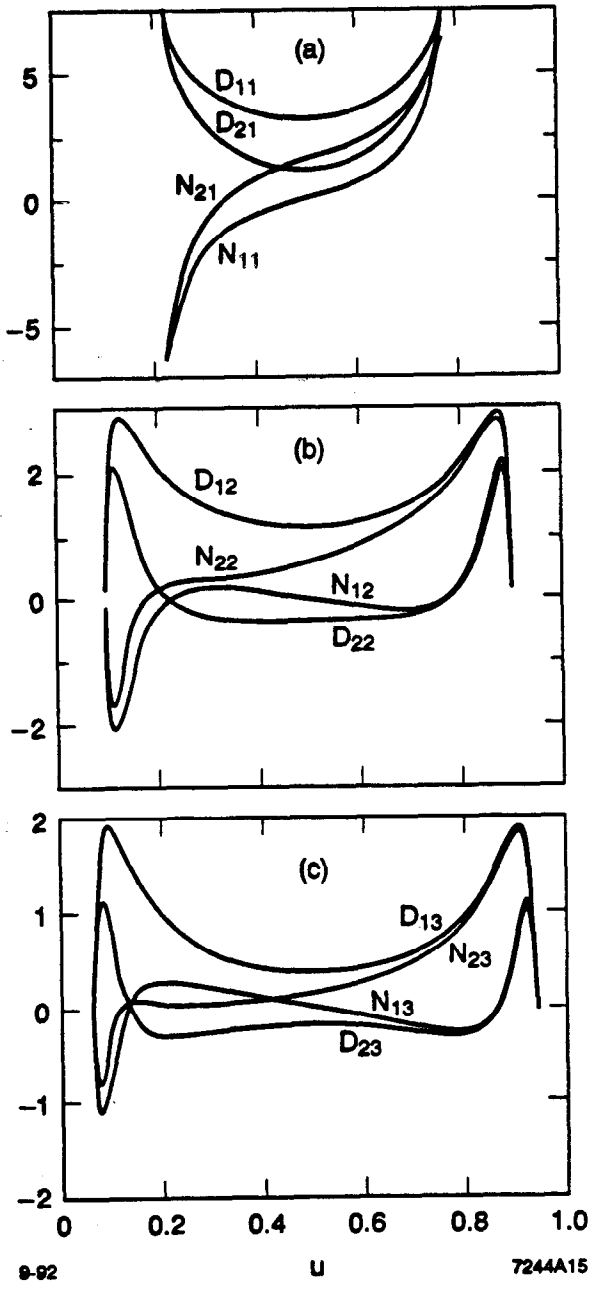
(a)
5
0
−5
D_{11}
D_{21}
N_{21}
N_{11}
(b)
2
0
−2
D_{12}
N_{22}
N_{12}
D_{22}
(c)
2
1
0
−1
−2
D_{13}
N_{23}
N_{13}
D_{23}
0
0.2
0.4
0.6
0.8
1.0
u
9-92
7244A15

Fig.15

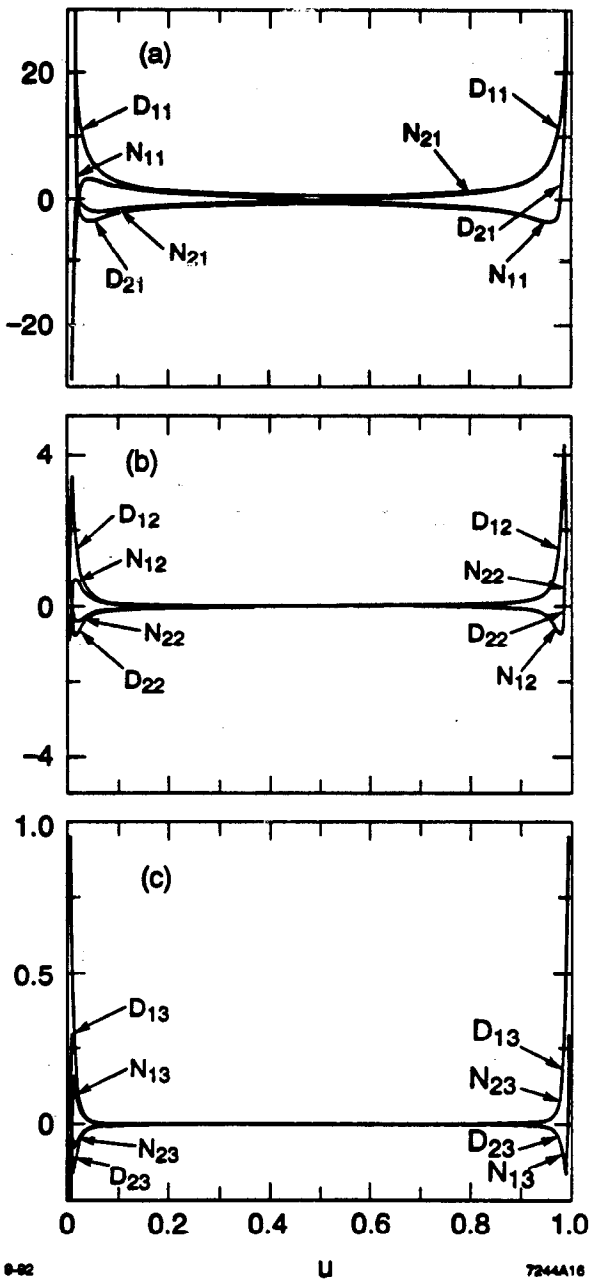
(a)
20
0
-20
D11
N11
N21
D21
D11
N21
D21
N11
(b)
4
0
-4
D12
N12
N22
D22
D12
N22
D22
N12
(c)
1.0
0.5
0
D13
N13
N23
D23
D13
N23
D23
N13
0
0.2
0.4
0.6
0.8
1.0
u
8-92
7244A16

Fig.16

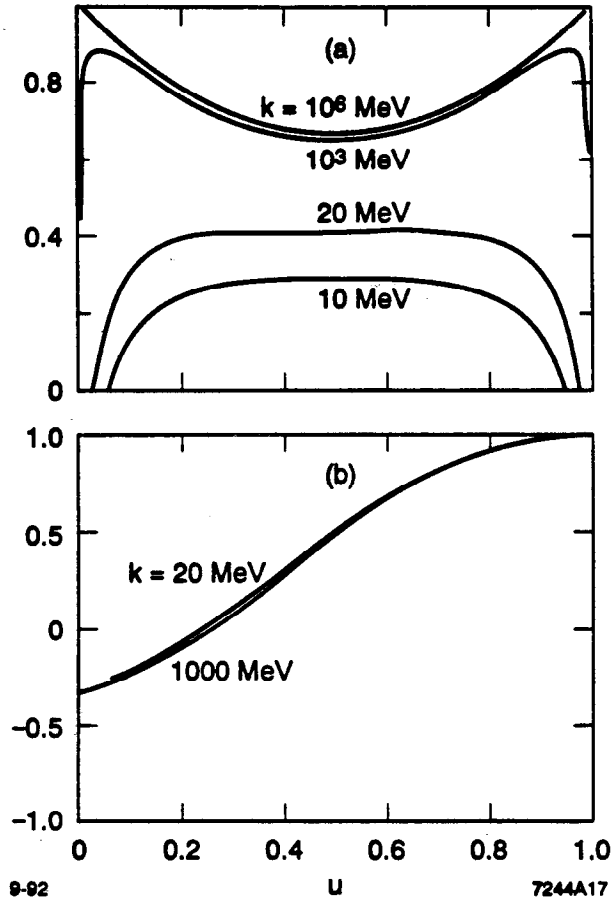
(a)
k = 10⁶ MeV
10³ MeV
20 MeV
10 MeV
0.8
0.4
0
(b)
k = 20 MeV
1000 MeV
1.0
0.5
0
−0.5
−1.0
0
0.2
0.4
0.6
0.8
1.0
u
9-92
7244A17

Fig. 17